

CHARACTERIZATION OF DIRECT PRINT ADDITIVE MANUFACTURING
PROCESS FOR 3D BUILD OF A CARBON NANOSTRUCTURE COMPOSITE

RICARDO XAVIER RODRIGUEZ

Department of Electrical and Computer Engineering

APPROVED:

Kenneth H. Church Ph.D.

Raymond C. Rumpf Ph.D.

Alexander B. Morgan Ph.D.

Charles Ambler, Ph.D.
Dean of the Graduate School

This Thesis is dedicated to the United States of America.

CHARACTERIZATION OF DIRECT PRINT ADDITIVE MANUFACTURING
PROCESS FOR 3D BUILD OF A CARBON NANOSTRUCTURE COMPOSITE

by

RICARDO XAVIER RODRIGUEZ, B.S.E.E.

THESIS

Presented to the Faculty of the Graduate School of

The University of Texas at El Paso

in Partial Fulfillment

of the Requirements

for the Degree of

MASTER OF SCIENCE

Department of Electrical and Computer Engineering

THE UNIVERSITY OF TEXAS AT EL PASO

August 2014

UMI Number: 1564696

All rights reserved

INFORMATION TO ALL USERS

The quality of this reproduction is dependent upon the quality of the copy submitted.

In the unlikely event that the author did not send a complete manuscript and there are missing pages, these will be noted. Also, if material had to be removed, a note will indicate the deletion.



UMI 1564696

Published by ProQuest LLC (2014). Copyright in the Dissertation held by the Author.

Microform Edition © ProQuest LLC.

All rights reserved. This work is protected against unauthorized copying under Title 17, United States Code



ProQuest LLC.
789 East Eisenhower Parkway
P.O. Box 1346
Ann Arbor, MI 48106 - 1346

ACKNOWLEDGEMENTS

First and foremost, I would like to thank Kenneth H. Church, my advisor, for the unparalleled passion, vision, and support that he has provided me over the years. With his guidance and encouragement, there is no way I would be as engaged or as passionate about my career and work. I would probably still be rummaging through the forest if it wasn't for your leadership and vigor. Thank you.

Thank you, Raymond C. Rumpf for kind patience and superior tutorship. The ideas and teachings you have bestowed upon me have inspired invigorated my curiosity and truly made time in El Paso worthwhile. You are on the very cutting edge of your discipline and a world class researcher; it was a true honor to be able to learn from you.

Alexander Morgan Ph.D., thank you for your support and professionalism throughout this endeavor. You have been patient, understanding, and insightful, and I ever so appreciate it. To your colleagues at the University of Dayton Research Institute, Kathleen A. Schenck and Scott A. Gold Ph.D., I thank and appreciate your contributions to this project.

Thank you to W.M. Keck Center for Three Innovation at University of Texas at El Paso. Namely Dr. Ryan B. Wicker, Dr. Francisco Medina, Dan Muse, and David Espalin Without the use of the facilities all of you maintain and your helpfulness throughout my experience there this project would never have happened. The facilities and people there are truly unique and I am proud and thankful to have been a part of the center's prestigious reputation.

To everyone at nScript and Sciperio, in Orlando, FL, I appreciate all the help you have provided to me, not just for this project but over the years. Harvey Tsang and Dr. Paul Deffenbaugh, your friendship and help during this work have been invaluable.

Finally there is no accomplishment I can take credit for without acknowledging my parents; Marco Antonio and Ana Maria Rodriguez. They created a life for me where I can pursue whatever passion my heart conjures. For this I am eternally grateful.

EXECUTIVE SUMMARY

This project is a focus on characterizing the process for actualizing three dimensional structures out of a carbon nanostructure composite via a direct print additive manufacturing process. Manufacturing parts additively enables for realization of geometrically complex shapes that often times cannot be manufactured any other way. The specificity of a material's properties have to be such, that the processing method can precisely place and bond material to itself in a highly repeatable manner. Commercial materials for additive manufacturing are have been optimized with these goals in mind and, therefore, often times lack the rigor and robustness for many applications.

The addition of nanomaterials is promising approach to enhance certain properties of AM materials without drastically altering their critical processing characteristics. This study looks into the reinforcing a commercial Stereolithography resin (DSM Somos™ Watershed 11122) with two types of carbon nanostructures (multi-walled carbon nanotubes and carbon nanofibers) in an attempt to improve mechanical characteristics of the bulk material. Related work has shown to not exceed concentrations over .5% (w/v) such that the material is still compliable with the AM technology. This study attempts to exceed these loading ratios, by attempting concentrations of: 1) 1% (w/v) 2) 2.5% (w/v) 3) 5% (w/v) 4) 10% (w/v).

A direct write system from nScrypt Inc. (Orlando, FL) is implemented as the extrusion method for the nanocomposite materials. An ultra-violet emitting radiation source is paired up with the nScrypt tool form a direct print additive manufacturing process that dispenses material then cures it right after. All the different processing characteristics and control variables are explained in great detail, as well as the design considerations for fabricating a part with this

technique. The impact of the control parameters to dispensed features are observed and measured. Statistical data is generated from this for the design of parts to be built with the system.

Test specimens for mechanical evaluation are designed based off of the parameter measurements and observation of the material within the system. The test specimens are built from the different nanocomposite concentration and a control sample are evaluated until failure under tensile loads. The fractured specimens are imaged under a scanning electron microscope to analyze layer interfaces and fracture characteristics. A thermal evaluation with photo-DSC is done on the materials to document their behavior under elevated temperatures ($0^{\circ}\text{C} - 300^{\circ}\text{C}$).

Background on the technologies, materials, and processes is provided first. A through discussions general AM workflow, technology, and history is given. Then a focus into pertinent technologies (Stereolithography) is discussed in detail. A breadth of direct write technologies and applications are introduced with an emphasis in the one (nScript, DPAM) utilized in this study. Finally, carbon nanostructures are introduced.

TABLE OF CONTENTS

ACKNOWLEDGEMENTS.....	iv
EXECUTIVE SUMMARY	vi
TABLE OF CONTENTS.....	viii
LIST OF TABLES.....	xi
LIST OF FIGURES	xii
CHAPTER 1 INTRODUCTION.....	1
1.1 MOTIVATIONAL BACKGROUND.....	1
1.2 MOTIVATION	3
1.3 OBJECTIVES	4
CHAPTER 2 BACKGROUND.....	5
2.1 INTRODUCTION.....	5
2.2 ADDITIVE MANUFACTURING.....	5
2.2.1 History.....	5
2.2.2 Technology Overview.....	9
2.2.3 Digital Workflow	11
2.2.4 Stereolithography.....	16
2.2.4.1 Technology Overview	16
2.2.4.2 Photopolymerization.....	17
2.2.4.3 Material Properties	19
2.2.5 Direct Write	22
2.2.5.1 History	22

2.2.5.2	Technology Overview	23
2.2.5.3	Direct Print Additive Manufacturing.....	26
2.2.5.4	Applications.....	27
2.3	NANO-COMPOSITES	29
2.3.1	Carbon nanotubes.....	29
2.3.2	Carbon Nanofibers	31
2.3.3	Polymer Carrier.....	32
2.3.4	Nano-Composites Research in AM	33
CHAPTER 3 EXPERIMENTAL SETUP AND METHODOLOGIES		35
3.1	INTRODUCTION.....	35
3.2	NANOCOMPOSITE MATERIAL	35
3.2.1	Polymer Carrier.....	36
3.2.2	Carbon Nano-Tubes	37
3.2.3	Material Mixing	38
3.2.3.1	Material Loading	39
3.3	DPAM SYSTEM DESCRIPTION.....	40
3.3.1	nScript System Overview.....	40
3.3.1.1	Dispense Mechanics	42
3.3.1.2	Dispense Parameter Description.....	44
3.3.2	Ultra – Violet Curing Apparatus.....	46
3.3.3	DPAM Printing Procedure	49
3.4	SPECIMEN BUILD STRATEGY	51

3.4.1	Part Construction Methodology.....	51
3.4.2	CAD Design.....	52
CHAPTER 4	EXPERIMENTAL RESULTS AND OBSERVATIONS.....	55
4.1	SPECIMEN CONSTRUCTION.....	55
4.1.1	Line Width Measurements.....	55
4.1.2	Line Thickness Measurements.....	56
4.1.3	Specimen Build Results.....	57
4.2	MECHANICAL EVALUATION.....	60
4.3	FRACTURE IMAGING.....	63
4.4	THERMAL EVALUATION.....	66
CHAPTER 5	CONCLUSIONS.....	69
5.1	SUMMARY.....	69
5.2	FUTURE WORK.....	70
APPENDIX A	72
APPENDIX B	78
APPENDIX C	79
REFERENCES	81
CURRICULUM VITAE	88

LIST OF TABLES

Table 2-1 Categorical summary of AM modalities cross-referenced with materials; modified from Ref [35].	10
Table 3-1 Material properties of DSM Somos® Watershed™ XC 11122, adopted from Ref. [81]	36
Table 3-2 Nanocomposite concentrations given as percentage of solute weight by volume.	38
Table 3-3 List of system control paramters.	44
Table 3-4 List of print parameters settings used to dispense the line characterizations	52
Table 4-1 Thicknesses of lines dispensed at the parameters in Table 3-4 and at a dispense gap of 70μm.	57
Table 4-2 Statistics for change in layer thickness measurements	59
Table 4-3 Measurements of the photo-DSC measurements	68

LIST OF FIGURES

Figure 1-1 Parts fabricated with different additive manufacturing technologies: (clockwise) Electron Beam Melting, Stereolithography, Fused Deposition Modeling	2
Figure 2-1 Counter lines of relief map as originally published in the Blather patent [23].	6
Figure 2-2 First parts fabricated with experimental SLA systems; Kadoma (left), Herbert (right)	7
Figure 2-3 Chronology of additive manufacturing as discerned by Ref. [4].	8
Figure 2-4 Breakdown of AM technologies by feedstock type to processing technology to modality; modification of Ref [36].	11
Figure 2-5 Conversion of solid part to STL file.	13
Figure 2-6 Left: Example of part getting sliced into discrete layers. Right: Example of layer fill pattern.	14
Figure 2-7 Stereolithography Apparatus schematic	17
Figure 2-8 Schematic for the free radical photopolymerization process, modified from Ref [40].	18
Figure 2-9 Beam profile for SL laser.	20
Figure 2-10 Example of working for a commercial SL resin, DSM Somos® Watershed™ 11120; [12].	21
Figure 2-11 Example of awkward, conformal antenna on a honeybee’s abdomen; from Ref [11].	27
Figure 2-12 Concept of embedded sensors and integrate electronics, from Ref [11].	28
Figure 2-13 Representation of CNT embedded in a polymeric matrix [65].	29

Figure 2-14 a) Single walled CNT imaged with TEM b) Multi-walled CNT imaged by TEM, scale bar of 5nm. As shown in Ref [68].....	31
Figure 2-15 Comparison of different carbon tubules structures, modified from Ref. [74].	32
Figure 3-1 Components used to loaded syringe.....	40
Figure 3-2 Typical nScript deposition system configuration.....	42
Figure 3-3 SmartPump™ hardware schematic	43
Figure 3-4 Open and closing mechanism for the nScript SmartPump™	44
Figure 3-5 Illustration of dispense common dispense scenarios, modified from [85].....	46
Figure 3-6 Relative intensities of the PC 1000F bulb across UV spectrum (courtesy of American Ultraviolet).....	47
Figure 3-7 Nanocyl 1% (w/v) after ~5 seconds of the exposure at 400 W/in ²	48
Figure 3-8 (A) Temperature measurement set up (B) Temperature variations of cure stage on 'low' setting.	49
Figure 3-9 DPAM process station; (A) UV curing apparatus (B) nScript build platform.....	50
Figure 3-10 Topological scan visualization of the vacuum chuck area where parts were built ...	51
Figure 3-11 Pen tip dimensions used throughout study.....	52
Figure 3-12 (A) Design mechanical test specimen (B) 90 degree orientation (C) 0 degree orientation	53
Figure 3-13 (A) Overlap = 0 (B) Overlap = .1 (C) Overlap = .25	54
Figure 4-1 Plot of averaged line widths vs. dispense gap.....	56
Figure 4-2 Graph of each layer's thickness	59
Figure 4-3 Optical imaging of the mechanical test specimen with width measurements.....	60

Figure 4-4 Stress-Strain curve generated from the Somos™ Watershed 11122 mechanical evaluations	61
Figure 4-5 Stress-Strain curve generated from the mechanical evaluations of the nanocomposite variations.....	62
Figure 4-6 Stress – strain comparison between all mechanical specimen.....	63
Figure 4-7 Cross sectional view of a Nanocyl 1% (w/v) fractured specimen; at 45X magnification.....	64
Figure 4-8 Cross sectional view of a Nanocyl 2.5% (w/v) fractured specimen; at 47X magnification.....	65
Figure 4-9 Cross sectional view of a Nanocyl 5% (w/v) fractured specimen; at 187X magnification.....	66
Figure 4-10 Cross sectional view of PR-24 5% (w/v) fractured specimen; at 1,112X magnification.....	66
Figure 4-11 Photo-DSC output of DSM Somos™ Watershed 11122	67

CHAPTER 1 INTRODUCTION

1.1 MOTIVATIONAL BACKGROUND

The first industrial revolution was started in Britain in the mid-eighteenth century. It was mainly centered on the textiles industry. The idea was simple; set up a facility that could reproduce single textile repetitively. This practice was soon then adapted to other industries (e.g. glass making, construction, paper). Driven by technological advances, the revolution in how to make things opened the door for designers to meet the needs of the market. Soon after another industrial shift, known as the “second industrial revolution” took place [1]. This time the shift in manufacturing was driven by the need for transportation. Railroads made it cheap for materials to be transported over long distances. The advent of the automobile and its manufacturing line invigorated a nation. Industries such as steel production, electricity, and petroleum soon after emerged to meet these demands.

Always technologically driven, the two industrial revolutions were both focused on replicating a single design over and over again. Products that are produced in such a fashion are really designed for being fabricated over and over again, thus constraining the designer. Large, elaborate facilities are set up to make something over and over again, rather than being tailored to meet the specifications for the exact end use deliverables [2]. Designs also have to be retrofitted for assembly because often multiple materials with drastically different processing schedules are needed to be combined. This makes designing something that is unique and complex very difficult and expensive.

The third industrial revolution is slate to change that [3]. The adoption of the additive manufacturing techniques has shown to be a promising avenue for solving the obstacles of the

diversifying and customizing product designs, that traditional manufacturing methods have. Additive manufacturing is a confluence of materials processing, computer aided design (CAD), and control robotics, which will potentially enable the designer to shrink the logistics chain and deliver parts to the end user more expediently and customized to their needs. By selectively ‘adding’ material where needed, part costs and waste can be reduced. Large, expensive manufacturing facilities will begin to disappear. Engineers and designers will essentially create products in digital formats that an end-user can later purchase, modify, and upload into his or her personalized manufacturing tool.

The idea of having a personalized factory is becoming more and more realistic. Desktop fabricators (i.e. 3D printers) can now be purchased to fabricate three-dimensional models very readily. While these printers are dominated by thermoplastics, more production-end equipment has emerged that enable users to produce complex, fully customizable parts out of metals, ceramic, and thermosetting resins. Figure 1-1 displays parts manufactured with different additive manufacturing modalities.

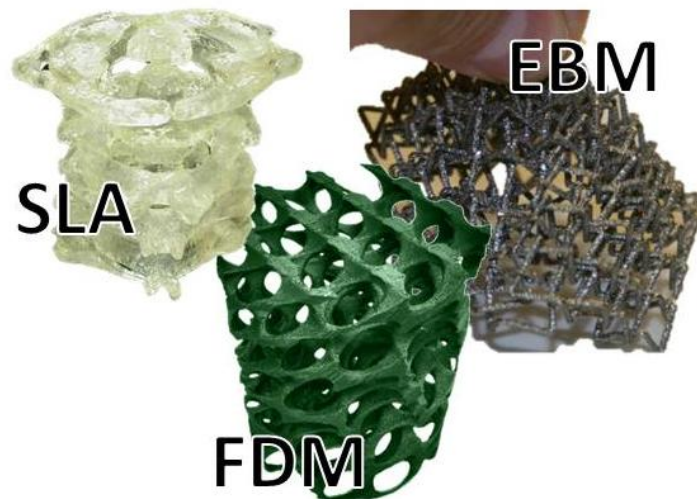


Figure 1-1 Parts fabricated with different additive manufacturing technologies: (clockwise) Electron Beam Melting, Sterolithography, Fused Deposition Modeling

While additive manufacturing technologies have been around since the early 1980's [4] most of the technologies are only capable of producing parts of one material at a time. This then drastically limits a designer to just producing models or prototypes of the actual parts. In order for these technologies to go from just producing prototypes or models of the end use products the following must happen: 1) materials of drastically different properties must be processed within a single tool environment 2) the final part realized must go through no assembly process.

1.2 MOTIVATION

The use of carbon nanostructure of has drastically increased in recent years because of the unique properties they exhibit [5, 6, 7, 8, 9]. One of their most promising benefits are the superior mechanical properties that have been observed; up to 63 GPa [8]. Their small structures (nanometers wide) and high surface area (e.g. 300 m²/g) in a bulk state allows for the high affinity and interaction within a suspending matrix. This approach to material reinforcement is already one widely accepted within the traditional composite materials industries, such auto racing and aerospace. In those industries, fiber systems (i.e. carbon, glass, Kevlar®) are arranged in specific orientations and patterns to achieve certain mechanical properties [10]. However, conventional manufacturing techniques are slow, expensive, and expertise in processing.

Additive manufacturing (AM) technologies are poised to remedy this conundrum. Current additive materials lack the mechanical requirements for applications outside of household objects or show models [11]. Many of the materials that are used for AM processes are tailored to being able to process them in very effective and repeatable manners, with little concern for mechanical integrity. The introduction of carbon nanostructures has the potential to enhance AM material

properties (i.e. mechanical) with drastically altering the properties that makes suitable for an AM technology.

Sandoval et al. [12, 13] has been successful in processing and enhancing Stereolithography (SL) resins with carbon nanostructures. However, the concentrations of used were very low (<.5% (w/v)). Low carbon nanostructure loadings were necessary in that instance because of their impact on the aggregate's rheological properties. Higher concentrations would have rendered the material inadequate to process through a SL system. Therefore, a new technique is required that can accurately ($\pm 1\mu\text{m}$) process a carbon nanostructure loaded composite high, relative concentrations (<1% (w/v)) in a repeatable manner.

1.3 OBJECTIVES

This project's objective is to then characterize and develop a process for constructing a three dimensional object out of a carbon nanotube-epoxy based resin (DSM SomosTM WaterShed 11122) composite via a Direct Printed Additive Manufacturing (DPAM) dispensing system. To meet this over-arching objective, the following must be accomplished:

1. Characterize the dispensing parameters of the different CNT-resin loading (by volume) combinations and determine the reproducible dispense dimensions.
2. Characterize the cure rate of the different composite combinations.
3. Fabricate tensile test specimens and contrast the different loadings with each other for mechanical performance; as well as comparing this specimen to an unfilled test specimen.
4. Image the fractured specimen under SEM to get a detailed dimensional analysis of the part construction.

CHAPTER 2 BACKGROUND

2.1 INTRODUCTION

This chapter gives a comprehensive introduction to technical areas that are involved in this study and further supplement the need for this work (as described in chapter 1). Additive manufacturing terminology is defined and overview of its history and contemporary technologies are given. The work carried out in this project revolves around a commercially available resin utilized in Sterolithography systems and a deposition technology traditionally used in Direct Write application. Therefore, detail on the two technologies is given. Nanotechnology is introduced with emphasis of carbon nanotube (CNT) technology, its properties, and applications that are pertinent to this study.

2.2 ADDITIVE MANUFACTURING

2.2.1 History

Additive manufacturing (AM) is defined by the ASTM subcommittee F42.91 [14] as, “a process of joining materials to make objects from 3D model data, usually layer upon layer, opposed to subtractive manufacturing methodologies”. In other words, it is a technique or approach for fabricating an object rather than reference to specific technology. There are many subsets, or modalities that can fabricate parts in an additive way. These technologies are capable of producing full three dimensional objects made out of polymers [15, 16], ceramics [17, 18], metals [17, 19, 20] and several combinations thereof [17]. In more recent years, AM technologies have even extended to the deposition of biological tissues [21, 22]. Regardless of

the distinction in materials or processing science, the commonality in all these technologies is the link between software and hardware. All parts fabricated in an AM modality is designed in a computer aided design (CAD) software then is processed to be fabricated additively.

Part of the definition of an AM process, as described in the previously, is the layer based approach [14]. A review of the patent literature done in Ref. [4] elucidates two technologies that predate modern, digital approaches to additive manufacturing; topography [23, 24] and photosculpture [25]. Relief maps could be constructed by cutting out contour lines out of cardboard then sequentially stacking them on top of each other. The process of stacking of sequentially stacking contoured layers as patented by Blanter is shown in Figure 2-1.

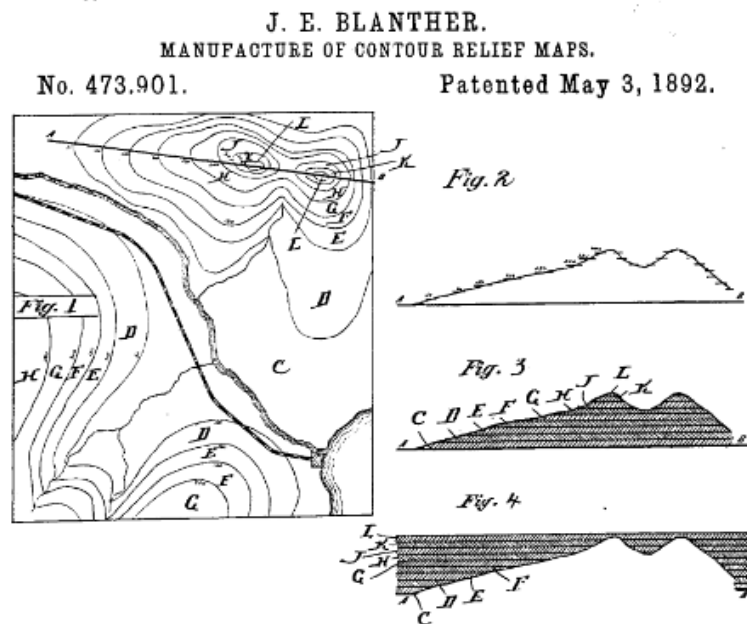


Figure 2-1 Counter lines of relief map as originally published in the Blanter patent [23].

Later, more patents emerged in the field of topography. More materials began surfacing employing photo-curable resins that served as the adhesion mechanism for the topographical layers [26]. Combinations of photosculpture and topography were also implemented as early as

1935. In this method, light was used to cast contour lines of an object that could then be developed into sheets, later cut and stacked [27, 28].

Forming technologies began to resemble modern AM technologies with filing of the Swaisson patent in 1968 [29]. This machine would cross-link a photosensitive polymer with two intersecting energy sources. This system began the evolution of photosculture into additive manufacturing by having the energy direction be computer controlled. Herbert [30] and Kodama [31] showed the first fabricated parts through stereolithography in 1982 and 1981, respectively. Shown in Figure 2-2 are the originally published parts, as shown in Ref. [4].

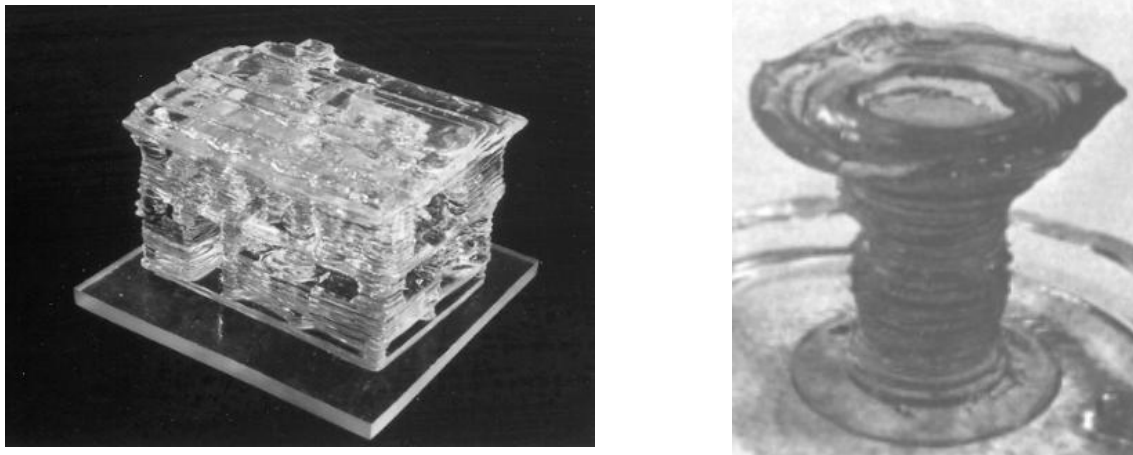


Figure 2-2 First parts fabricated with experimental SLA systems; Kadoma (left), Herbert (right)

Soon after the Herbert and Kodama publications, a wave of AM patents sprung up in the 1980's and 1990's. Companies focused on manufacturing AM equipment began to form and an industry was born. The first and arguably most famous was Chuck Hull's patent of the Stereolithography Apparatus (SLA) in 1984. He soon then started 3D Systems in Valencia, CA and the first commercially available was shipped in 1988. That same year Scott Crump founded Stratasys, today's global leader in Fused Deposition Modeling (FDM). Stratasys soon filed the first patent for FDM the following year (1989). A few years before, 1986, a doctoral student at the University of Texas-Austin by the name of Carl Deckard filed the first patent for Selective

Laser Sintering of plastics and soon founded DTM (later acquired by 3D Systems). This technique would later be adopted by several as the fundamental process for fabricating metals components. The chronology of key moments in the history of additive manufacturing is shown in Figure 2-3.

TOPOGRAPHY		PHOTOSCULPTURE	
Blanthier patent filed	1890	1860	Willeme photosculpture
Perera patent filed	1937	1902	Baese patent filed
Zang patent filed	1962	1922	Monteah patent filed
Gaskin patent filed	1971	1933	Morioka patent filed
Matsubara patent filed	1972	1940	Morioka patent filed
DiMatteo patent filed	1974	1951	Munz patent filed
Nakagawa laminated fabrication of tools	1979		
	1968	Swainson patent filed	
	1972	Ciraud disclosure	
	1979	Housholder patent filed	
	1981	Kodama publication	
	1982	Herbert publication	
	1984	Maruntani patent filed, Masters patent filed, Andre patent filed, Hull patent filed	
	1985	Helisys founded Denken venture started	
	1986	Pomerantz patent filed, Feygin patent filed Deckard patent filed, 3D founded, Light Sculpting started	
	1987	Fudim patent filed, Arcella patent filed, Cubital founded DTM founded, Dupont Somos venture started	
	1988	1st shipment by 3D, CMET founded, Stratasys founded	
	1989	Crump patent filed, Helinski patent filed Marcus patent filed, Sachs patent filed EOS founded, BPM founded	
	1990	Levent patent filed, Quadrax founded, DMEC founded	
	1991	Teijen Seiki venture started Foeckele & Schwarze founded, Soligen founded Meiko founded, Mitsui venture started	
	1992	Penn patent filed, Quadrax acquired by 3D Kira venture started, Laser 3D founded	
	1994	Sanders Prototyping started	
	1995	Aaroflex venture started	
	1997	Aeromet formed, Optomec restarted, Z Corp started	
	1998	Objet founded	
	1999	POM founded, BPM closed	
	2000	Helisys closed, Solidica started	
	2001	3D and DTM merge	

Figure 2-3 Chronology of additive manufacturing as discerned by Ref. [4].

2.2.2 Technology Overview

It is first important to preface the following discussion by identifying the scope of scale that will be introduced. The accepted definition of additive manufacturing [14] can encompass broad range of techniques. This discussion will be limited to AM technologies that produce macroscopic parts (i.e. >1mm). Mesoscopic fabrication methods with nanometer precision [32, 33, 34] are outside of the scope of this study.

Additive manufacturing modalities are primarily classified by the material processing technique that each piece of equipment employs to produce a fabricated part. Currently the industry recognizes seven additive manufacturing processes: 1) Binder Jetting 2) Directed Energy Deposition 3) Material Extrusion 4) Material Jetting 5) Powder Bed Fusion 6) Sheet Lamination 7) Vat Photopolymerization. More distinction can be made within these categories by the type of materials that are processed. Furthermore, AM technologies can be distinguished by the dimensional accuracy of the produced part in comparison to its digital conceptualization of the part. Parts are said to be “near net shape” if they come within close enough tolerances of the desired geometrical features that little to no finishing is required. Net shape parts require post-processing steps (e.g. machining, grinding) to bring the part within the desired geometries. A categorical breakdown of commercial equipment based on the terminology found in Ref. [14] and cross-referenced with the materials processed is shown in Table 2-1 **Error! Reference source not found.**; the scope of the technologies shown is limited to “professional” quality printers.

Table 2-1 Categorical summary of AM modalities cross-referenced with materials; modified from Ref [35].

Category	Description	Polymers		Metals		Ceramics	
Binder Jetteing	Liquid bonding ink is selectively spread to join solid powder	ExOne	S-Print	ExOne	M-Print	3DS ExOne	ProJet S-Print
Directed Energy Deposition	Focused thermal energy melts material as deposited			Optomec* Sciaky* DM3D*	LENS EBW POM		
Material Extrusion	Material is selectively dispensed through a nozzle or extruder	Stratasys nScrypt	FDM 3Dn	nScrypt	3Dn		
Material Jetting	Droplets of build material are selectively deposited layer by layer	Stratasys	Objet	3DS	ProJet		
Powder Bed Fusion	Thermal energy selectively fuses regions of powder bed material	3DS	sPro	EOS 3DS	DMLS DMP	3DS	Voxeljet
Sheet Lamination	Material sheets are bonded together and selectivel cut in each layer to create desired 3D Object	Solido	SD 300	Fabrisonic*	SonicLayer		
Vat Photopolymer	Liquid photopolymer is selectively cured using a light source	3DS Envisiontec	iPro Ultra 3SP				

**Denotes near net shape technology*

It can also be useful to sort AM technologies by the form of the stock materials that are used to realize 3D parts. From that it is natural to break down the materials into how they are processed. This provides a better for map for selecting out of what material a part will be made. Based on the inherent characteristics of the processing science and the material, AM modalities can also be classified, or arranged by resolution. A system’s resolution metric can be thought as the amount of material that system can control during a part build. Equipment with high resolution are typically those that can control very small amounts of material (on the order of

micrometers) in all X, Y and Z directions. Figure 2-4 depicts the breakdown of AM modalities from stock material and attempts to show the range of resolution for specific types of equipment, while classifying by material.

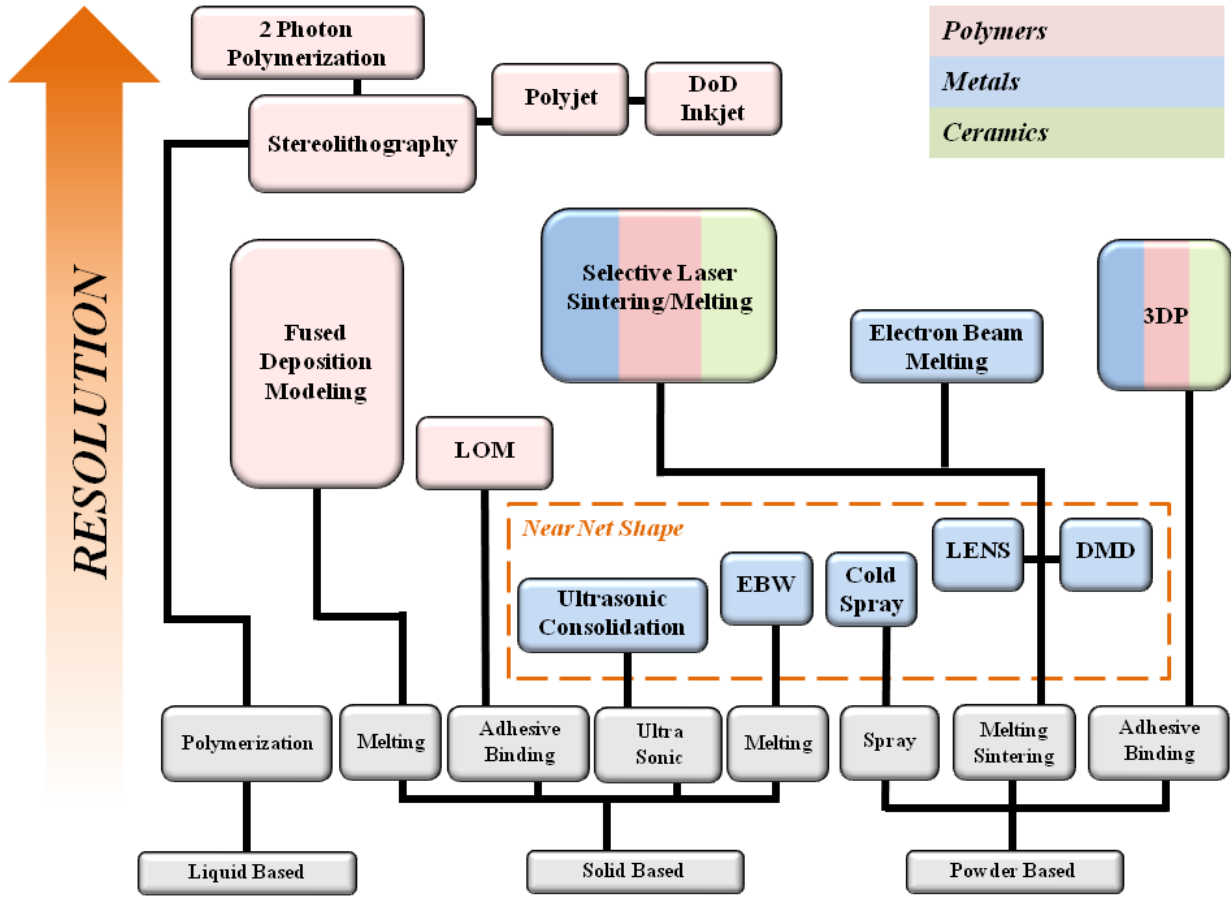


Figure 2-4 Breakdown of AM technologies by feedstock type to processing technology to modality; modification of Ref [36].

2.2.3 Digital Workflow

While there are a myriad of AM technologies available that are capable of processing things from polymers to ceramics, there is still one commonality between all of them: they all fabricate parts from CAD model. The process for this is the same across all modalities; the

differences come in how accurately the part gets fabricated in the end. Limitations are set by the system's resolution (*see 2.2.2*) and the software adjusts accordingly.

The process to realize a part with additive manufacturing takes approximately eight steps. This can depend on the specific material and equipment that is being used. The user's application may also require a part to be further treated to achieve some kind of enhanced performance or to better put the part within a certain specification. This will discussion will only focus on the steps that encompass all technologies.

The steps for fabricating a part with an additive technology can be summarized as follows [11]:

1. Generate computer aided design (CAD) of part.
2. Convert CAD model into an STL file.
3. Transfer STL file to AM Machine and manipulation.
4. Machine setup.
5. Build part.
6. Removal and cleanup.
7. Post-process
8. End-use application

A part is usually designed in CAD software package that gives you a three dimensional digital rendition of the actual geometries to be fabricated. There are numerous software packages available in the market place ranging from "hobby" level quality to high end "professional" level packages that are even capable of doing simulations and modeling. CAD software was first developed to give the designer a visual medium to which develop a part. Hence, geometries built in CAD are really what is thought of as a "solid part". Therefore, the "solid model" must be converted into an STL file (STereoLithography file).

The STL file was first developed by 3D Systems in the early 1990's and has since been adopted as the universal file for all AM technologies. It is a simple way of the representing a model with geometrical features alone. With an STL file a part is described by a series of triangles; essentially a mesh is created on the part's surface. Figure 2-5 shows the transition of a part from a solid model (or part) to the STL file. There are a number of issues with tessellating the surfaces of solid models (generating STL files). To correct STL files, there are software suites such as Magics™ from Materialise [37] that have specialized algorithms for correcting these errors. Further discussion on STL errors can be found in Ref. [11].

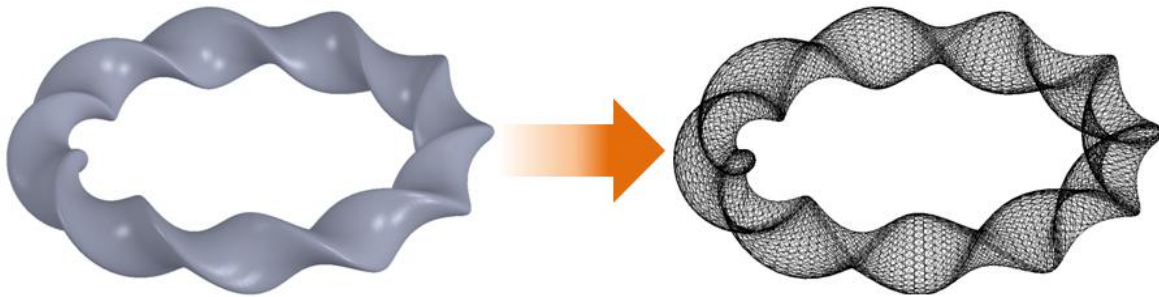


Figure 2-5 Conversion of solid part to STL file.

It should be noted that not all parts have features that can be freestanding during a build. To remedy this, an intermediary step where structures known as “supports” are created to hold the part during the build. Supports are also used to detach the part from the substrate it is being built on. This makes removing the part from the platform less painstaking and reduces the risk of damage that could be incurred during the removal. Software packages such as Magics™ have features for aggregating supports to parts represented as STL files. For basic geometries, it is often recommended that users build their own support structures as inherent part features at the CAD stage. However, more and more AM equipment manufacturers are incorporating automatic support feature generation in their equipment interfaces.

Once the STL files are ready, they are then transferred onto the AM machine environment. Most AM equipment of have a user interface that allows the user to position, orient, and create duplicates (supports for some manufacturers). It is at this stage that the user has a virtual representation of the parts that are going to be built in that run. The STL files are then “sliced” into discrete layers from the base of the build platform and towards the top of the tallest part in the build envelope. The nominal thickness of each of these layers is typically 100µm. However, this is dependent on the specific AM technology that will be fabricating the part. For example, the layer thickness for most FDM tools is 254µm, while SL layers can go down to 50µm thick layers. Each sliced layer is the filled with the paths of how the material will be deposited within each layer. The resolution of the fill pattern is set by each AM modality and the material being used for the build in some cases. It is usually predetermined and adjusted accordingly for the build. Figure 2-6 shows an example of sliced model and the fill pattern generated for a selected layer.

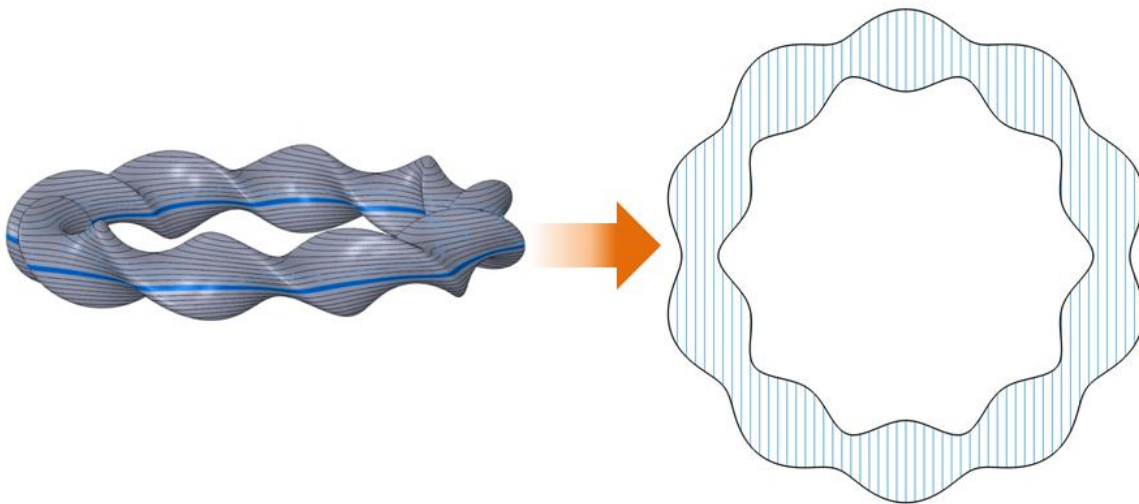


Figure 2-6 Left: Example of part getting sliced into discrete layers. Right: Example of layer fill pattern.

After the STL part is sliced and fill patterns are generate, it is ready to be uploaded into the AM machine. Certain fixtures and hardware setting on the machine platform has to be

adjusted accordingly to the actual build. In Stereolithography tools, for example, the energy source needs to be warmed up and calibrated, the resin level in the vat needs to be adjusted, and other hardware considerations need to be made before the build is initiated. Once the tool is setup, the build commences. The amount of time at this step varies for each AM modality and can even be material dependent. Build time is primarily driven by the height of the part as it is positioned on the build platform, as well as how resolved the individual layers are sliced. Regardless of time, the build stage should require little supervision.

Parts are nearly ready once the build is over. Support structures are typically need to be removed for completion. Depending on the AM modality (or material) supports are often removed in different ways. Stereolithography builds support structures with the same material that is used to build the part. They are typically weak structures that can easily be removed. Selective laser melting systems that build parts with metals use the same strategy, however, because the supports are made of consolidated metal, require a more intensive process. In contrast, FDM tool, especially those from Stratasys [38] use a thermoplastic that dissolves in a specific solution.

Before the part can be put into its intended use some post-processing may be require. This could mean at times sanding, polishing, or even metal plating. For example, Bae et al [39] has manufactured ceramic parts in SL with a novel ceramic nanocomposite. The AM system was used in this case to make a green part (pre-fired part) then consolidated in a furnace.

2.2.4 Stereolithography

2.2.4.1 Technology Overview

Stereolithography is an additive manufacturing technology that is classified as a ‘vat photopolymerization’ technology, per the ASTM 2792 standard [14]. It produces three dimensional parts by curing (i.e. solidifying) discrete layers of a photo-active resin (contained in a vat) with a radiating energy source, typically emitting an ultra-violet wavelength. Radiation of a certain power and particular wavelength emanates from a laser and passes through a safety shutter mechanisms. From there the beam is expanded by telescoping optics in order to increase its focal length. After being expanded, the radiating energy is directed onto two steering mirrors that rotate orthogonally to each other and scan the energy in the cross section pattern of the sliced layer. The energy is then focused and cures the material onto a build platform. When a layer is complete, the platform submerges into the vat and a recoating blade squeegees a new layer over the built part. The platform then rises stopping at a distance from the level line of the resin that is equivalent to that the layer thickness. The schematic of a SL system is shown in Figure 2-7.

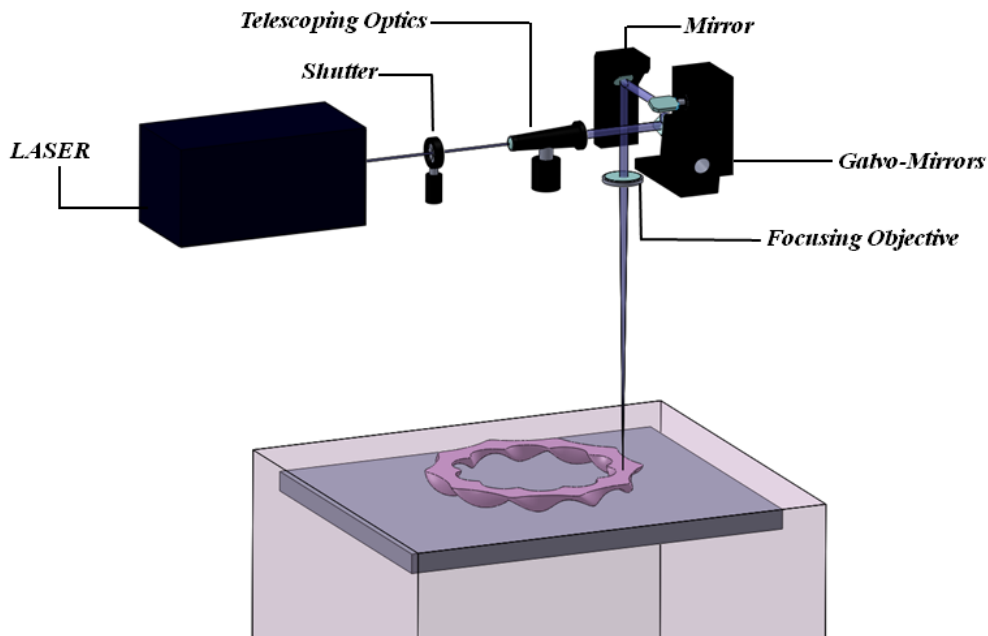


Figure 2-7 Stereolithography Apparatus schematic

2.2.4.2 Photopolymerization

The foundation of Stereolithography is the chemical process of polymerization. Essentially, polymerization describes the process of linking small molecules (monomers) together to form larger molecules (polymers) [40]. A monomer is said to be multifunctional if it can react and attach itself to other molecules; this is known as a cross-linking polymer. Liquid polymer systems begin to turn into solid systems as the distance between polymer groups decreases, while density and shrinkage of the material increases. There are currently two photopolymerization chemistries available: 1) free radical systems 2) cationic systems.

A free radical polymerization process is initiated by introducing a catalyst to bond monomer groups at reasonable rates. A combination of monomers can be combined with substance known as photoinitiators that react with photons [41] to release radicals, or molecule groups with free covalent bonds. Radicals that are formed attach to monomer groups in what is

known as the initiation phase. The monomer-radical systems form a macroradical, which is a monomer system with and free covalent bond. During the propagation phase macroradicals continue to react with neighboring monomers until termination. The polymerization chain reaction can end in three ways: 1) recombination 2) disproportionation, 3) occlusion. A recombination termination involves two radical systems reacting with one another to form a nonreactive molecule. Disproportionation is a process when two radicals react with one another without forming a polymer chain. The third termination method, occlusion, describes when a macroradical gets entrapped within the polymer network. Radicals can continue to propagate within a cure part, without exposure, for up to several months. This could contribute to shrinkage and warping of part of over time. Figure 2-8 depicts a schematic for the photopolymerization process. Here the M represents a monomer group, I a photoinitiator group and the \diamond symbol is indicative of a free radical.

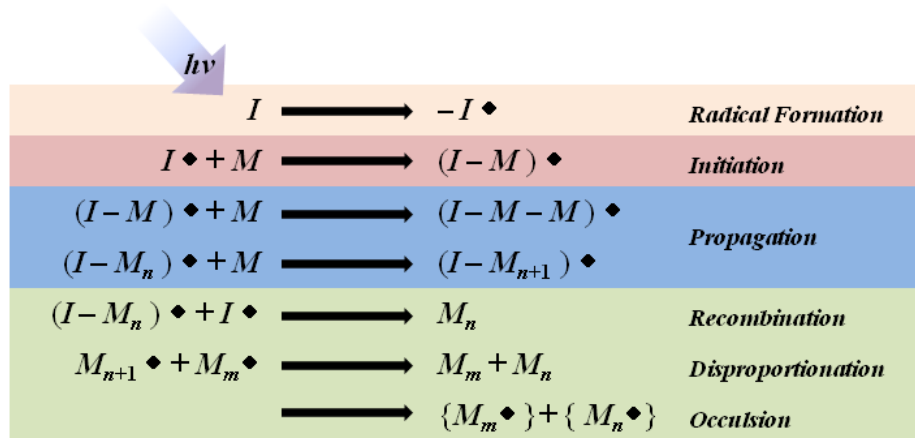


Figure 2-8 Schematic for the free radical photopolymerization process, modified from Ref [40].

Much like the free radical polymerization process, the cationic process involves the same steps to create polymer chains. Radiated energy is used to catalyze the polymerization process, forming a chain reaction of monomer chain bonding to one another. Finally, reaching a termination stage where the reaction is inhibited. The main difference between the two

processes is the type of photoinitiator chemistry that the two systems employ. Cationic initiators will react with a monomer system by inducing a charge to it. This now charged monomer reacts with neighboring monomer to further progress the reaction [42]. Initiators for cationic reactions are typically triarylsulphonium salts [11], however, secondary reactions may be induced by the reacted species present in the resin.

The monomers used for cationic reactions are epoxide or vinyl ether compounds, as opposed to free radical systems which utilize acrylate monomers. Acrylates form long polymer chains that aggregate with one another during the polymerization process. These networks can continue to react with either one another or entrapped radicals (through occlusion). Therefore, parts fabricated with these chemistries may experience shrinkage or warping over time. Epoxy systems, on the other hand, react by breaking up the epoxide's oxirane ring and then joining. This phenomena is more local than that exhibited by acrylate networks and thus forms a much more durable part. The free radical reaction is much faster mechanism than the cationic reaction. Therefore, contemporary SL resins are a combination of epoxy and acrylate networks.

2.2.4.3 Material Properties

Stereolithography systems build parts with a monochromatic (single wavelength) and coherent radiation source that outputs a Gaussian shaped energy profile as depicted in Figure 2-9. The maximum energy irradiate onto the surface of the resin is denoted as E_{\max} .

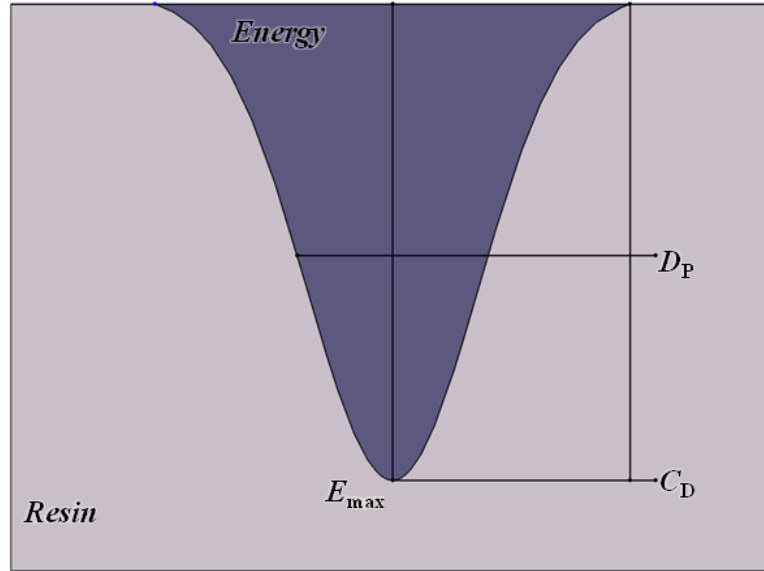


Figure 2-9 Beam profile for SL laser.

Resins for SL systems have two parameters that are inherent to each resin and need be accounted for when adjusting the proper build parameters. A resin's depth penetration (D_p) is defined as the distance radiated energy can penetrate into a resin before its irradiance is reduced by $1/e$ (or 66%); its units are given in millimeters. Critical exposure (E_c) is the amount of energy needed to initiate curing on the exposed of the resin. The cure depth (C_d) or the total distance energy will penetrate into the resin before it is quenched, can be written as function of these two parameters and can be determined by Equation **Error! Reference source not found.** (its derivation can be found in Ref [11]).

$$C_d = D_p \ln\left(\frac{E_{\max}}{E_C}\right) \quad (2-1)$$

Where E_{\max} is defined as,

$$E_{\max} = \left(\frac{P_L}{W_0 V_S}\right) \sqrt{\frac{2}{\pi}} \quad (2-2)$$

P_L is the irradiance of the laser (measure is watts), W_0 is the radius of the laser's beam waist on the surface of the resin (measured in millimeters), V_S is the scan speed of the laser (measured in millimeters per second).

A material's build parameters can be calculated out from generating parts and measuring their thicknesses; this determines the cured depth of the resin. Radiant exposure (E_{max}) is adjustable by the user by setting how fast the scan moves on the resin, the irradiance, the energy's beam waist. Therefore samples are built at different energy levels (usually by varying just the speed), their thicknesses are measured, then plotted against the respective exposure levels on a logarithmic scale. A linear regression is performed on the data to generate a working curve whose derivative with respect to exposure denotes D_p . The exposure value at which C_D is equal to zero (onset of polymerization) indicates the resin's critical energy, E_C . An example of a working curve for a commercial SL resin is shown in Figure 2-10. Sandoval [12, 13] et al. provides a detailed description of retrieving SL parameters from empirical analysis; the interested reader is highly recommended to read the cited sources.

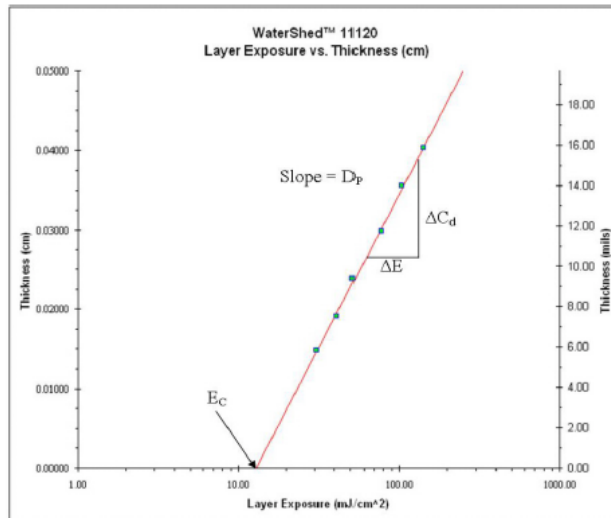


Figure 2-10 Example of working for a commercial SL resin, DSM Somos® Watershed™ 11120; [12].

2.2.5 Direct Write

2.2.5.1 History

Increased demands for the scaling down of the electronics sensors, devices, and MEMS in the commercial sector caused for conventional masking techniques to be made slow, inflexible, and nonforgiving [43, 44]. Direct write technologies began being developed as a means to address the issue of rapid fabrication of printed circuit boards at reduced costs and faster times [45]. Direct write technologies are far superior to conventional manufacturing techniques in terms of speed and turn around. Masking processes can take up to 24 steps to achieve a finished product [46]; a direct print process can take up to five [43]. Their drawback is in the quality and repeatability that can be achieved. Many of the direct print technologies are confined within the research and development community. Their high precision (millimeters) and ability to manipulate a myriad of materials at essentially no cost, has made the technologies very attractive for future development of novel processes.

Direct write technologies are a subset of additive manufacturing. In many ways it is thought of as micro-scale AM for unique materials and ultra high precision. The delineation between what is contemporarily thought of as “3D printing” and direct write is in the robustness of material that can be manipulated into scale. While, direct write technologies are mainly applied to small scale, one off applications there is potential for expanding them into larger applications, such as macroscopic part fabrication. The advances in materials will drive this effort as the vision for multi-material functionalization begins to transpire. Point-wise deposition of carefully selected materials will allow for the designer to tailor microstructural and

marcostructural features such as porosity, multi-material constructions, and graded interfaces [44].

2.2.5.2 Technology Overview

The review of direct write technologies described in the section is largely based on Ref. [44]. The reader is to refer to this reference for further details on technology, materials, and applications.

Direct write technologies are categorized into eight categories: 1) Plasma Spray 2) Laser Particle Guidance 3) MAPLE DW 5) Laser CVD 6) Micro Pen 7) Dip-Pen 8) Ink-Jet. These seven, describe particular technologies that are in current practice, however, several derivatives of these technologies being adapted to specific applications and materials across the research and development enterprise are constantly evolving the breadth of the industry. Mortara et al gives a comprehensive classification of direct write technologies that the interested reader is suggested to read [47]. Heule et al. further compares several direct write technologies and categorizes them by achievable resolution [48].

Plasma spray DW is a thermal spray technique. Typically a powder feedstock is heated by combustion generated from electrical current between a cathode and copper anode [49]. An inert gas that induces plasma enters from the rear section of the apparatus and flows through a vortex to the anode. An electric arc completes the circuit at the anode forming a plasma flame at the exit. Systems usually operate at the 40kW DC and introduce the powder feedstock at 15,000K. Plasma spray technologies can form down to 5 micron features with a range of materials that span from nickel and ferrous alloys to zirconia based ceramics.

Laser and flow guided direct write (LGDW) is a process in which colloidal inks containing small particulates (< 300nm in diameter) are aerosolized and fed into an optical path way. The LGDW device induces radiated energy operating at 1 W can induce up to 3 nN of force onto the particles in the direction of the beam. Energy scattering from the particles then generates forces that are perpendicular to the optical power, forcing the particles to the center of the beam. A hollow fiber is then used to guide the optical energy and particles over distances of several centimeters, blocking out any ambient disruptions that may overcome the delicate optical forces. Flow guided systems have an additional sheath air flow that is used to guide the particle stream through a sub-millimeter orifice that focuses down the particle stream further (about 5-10 times). Materials that can be processed with these systems range from metals to polyimides to ceramics; as long as it can be suspended into an ink. The different type of substrates is unlimited and resolutions are typically 2 – 25 μm . A post-processing routine is required (depending on the materials) to finalize the fabrication.

Matrix assisted pulsed laser evaporation (MAPLE) uses a focused pulsed of the radiated energy emitted in the ultraviolet spectrum to transfer a material held on a superstrate and onto the desired substrate. The material absorbs the incident energy, evaporating at the top interface and propelling the back face of the material onto the substrate into discrete features ($\sim 20 \mu\text{m}$). The resolution and performance that can be achieved is limited by the diffraction limit of the wavelength and the materials rheology, particle agglomeration, purity, and crystallinity. Matrix materials have rheological properties of inks and pastes ($\sim 1,000 - 100,000$ cps, respectively) and therefore can handle wide range of different types of materials.

Laser chemical vapor deposition (LCVD) is a process that utilizes a continuous wave (CW) laser to induce chemical reactions of molecules with absorptive substrates. Heat generated

from the laser catalyzes a gas containing metal molecules into pyrolysis at wavelengths absorbed by both the precursor and the substrate. The process is carried out in an enclosed chamber filled with the precursor material. Metal materials must have specific vapor pressure, stability, and decomposition activation energies in order to react efficiently.

Micro pen (or micro syringe) dispensing technologies are thought of as the most straightforward direct write systems. Material in ink or paste form is held in a reservoir and is forced with induced pressure through an orifice that can be as small as 12 μm . The dispensing apparatus is precisely controlled (state-of-art $\pm 1 \mu\text{m}$ [50]) by a gantry system that traverse a substrate to deposit a desired pattern. A wide range of materials can be accurately manipulated with these systems, materials up to 1,000,000 cps have been shown to be deposited with these systems. High repeatability in feature dimensions can be an issue due to transient pressure control at the beginning and end of deposition. Particle size distribution, morphology, and agglomeration can also lead to inconsistent results because of the filter pressing effects. However, these technologies are best suited to build structures with multi-functional materials at meso to macro scales [51, 52].

Dip pen direct-write (or dip pen nanolithography, DPN) systems allow for the transportation of molecules to a surface by the guidance of atomic force microscopic (AFM) tip. A meniscus of water at the tip of the AFM forms an interface with the substrate and provides a capillary driving for the molecules. Inks have to be designed properly such that their chemistries react with the substrate's surface to provide an added driving force to the molecules. DPN techniques can achieve feature sizes of 12 nm and with spatial resolutions of 5 nm. While slow, DPN can be parallelized to cover larger areas (micron range). Positioning feedback is needed to control the accuracy of motion at such small scales. Compared to the other direct write

technologies mentioned, DPN is still in its infancy. Formulations of inks compatible with various substrate types and meniscus transporters are still being developed.

Ink jet writing technologies are similar to the micro pen technologies in that they are non-contact methods where an ink is deposited on the substrate. However, the mechanism for deposition is in the form of a drop stream, therefore these systems are known as drop-on-demand (DoD) systems. They are attractive because of their compatibility with digital control and scalability. Ink jet systems work primarily with low viscosity (10 – 20 cps) inks and therefore, functional particulates are limited to being suspended in liquid carriers. Substrate selection is also crucial in that proper surface tension compatibility with the ink is required to avoid spreading. Volatile carriers are also important in that they allow for fast drying upon deposition.

2.2.5.3 Direct Print Additive Manufacturing

Direct Print Additive Manufacturing (DPAM) can essentially be thought of as a DW micro pen technique that has been extrapolated out of planar and conformal deposition applications to a third, continuous dimension. Work from Lewis et al [53, 54] has shown that three-dimensional structures can be constructed with DW systems as long as careful consideration of the modeling material is taken. Influential rheological properties such as viscosity, yield stress, and compression, as well as viscoelastic properties of shear loss and elastic moduli [53] must be tailored carefully to achieve repeatable control of three-dimensional construction. Interfacial bonding of material layers is also of great importance when lithographically extruding material in sequential layers. Current material technologies, outside of the thermoplastics (as in FDM), have been limited to the geometries that can be realized. Much success in the fabrication of mesoscale, periodic structures have been achieved [55, 56], however

the lack of complexity that is inherent to these structures simplifies processing considerations. For geometrical complexity to be introduced self-material surface tension, material mass, and inertia effects of the extrusion path need to be characterized in order to ensure repeatable and reliable deposition through the entire construction.

2.2.5.4 Applications

Development for direct write technologies flourished for the need to rapidly prototype electronic devices. Focus on electronics speed writing, materials quality, and processing temperatures is where the largest focus in development. DW technologies enable for the fabrication of electronic circuit board to be simplified and less of a financial burden [57]. Electronics integration with DW systems dominates the mesoscale range and bridges the gap between the integrated circuit world and the surface mount landscape ($> 10 \text{ mm}$). Examples of mesoscale devices such as multilayer battery assemblies and antennae have been much the focus of the DW community. Figure 2-11 depicts an example of an awkward antenna fabricated on the abdomen of a honey bee with a direct write.



Figure 2-11 Example of awkward, conformal antenna on a honeybee's abdomen; from Ref [11].

Tailoring of material properties have enabled for the improved performance of photovoltaic devices by achieving unique feature sizes [58]. Warren [44] states that the ability to conformally integrate passive and active electronic components on any substrate will: 1) modulate devices 2) 3) save space 4) become more robust 5) reduce fabrication lead time 6) reduce the cost of small batch production 7) fully integrate device with structure [59]. An example of the integrated mesocale electronics bonding with direct write is shown in Figure 2-12.

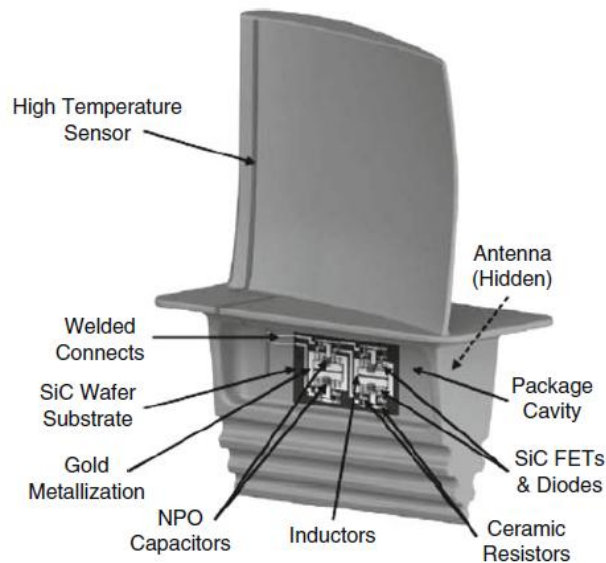


Figure 2-12 Concept of embedded sensors and integrate electronics, from Ref [11].

Other applications of direct write technologies include tissue engineering scaffolds [60], drug delivery devices [61], microfluidic networks [62], sensors [63], and photonic band gap materials [64]. The applications have implemented direct-write into specific applications because of the freedom of complexity and seamless integration with digitally aided control platforms. Specialized materials, as alluded to before, are at the center of the practices. Consideration for ink and paste properties, both functional and physical, as well as the introduction of hybridized techniques are key areas of future research for expanded applications and wide adoption.

2.3 NANO-COMPOSITES

Traditional composites are an aggregation of different materials that exhibit drastically different properties (e.g. polymers and ceramics) but arranged in such a way that they exceed the performance of either of its bulk constituents. An example would be adding carbon fibers to polymer matrices in order to improve mechanical and fracture properties [8]. A nano-composite is described as a material that consists of a matrix and a disperse nano-particulate that induces change to its overall macroscopic properties. A representation of a CNT embedded in a polymer matrix is shown in Figure 2-13 [65].

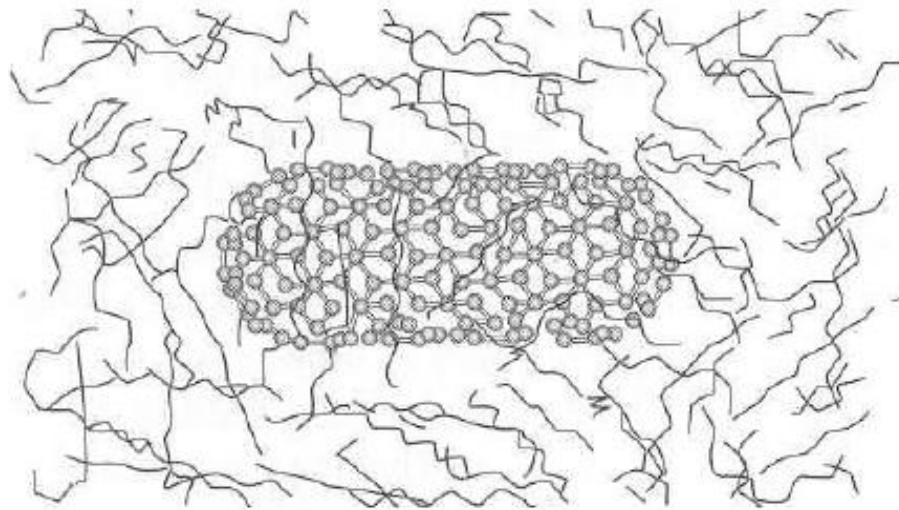


Figure 2-13 Representation of CNT embedded in a polymeric matrix [65].

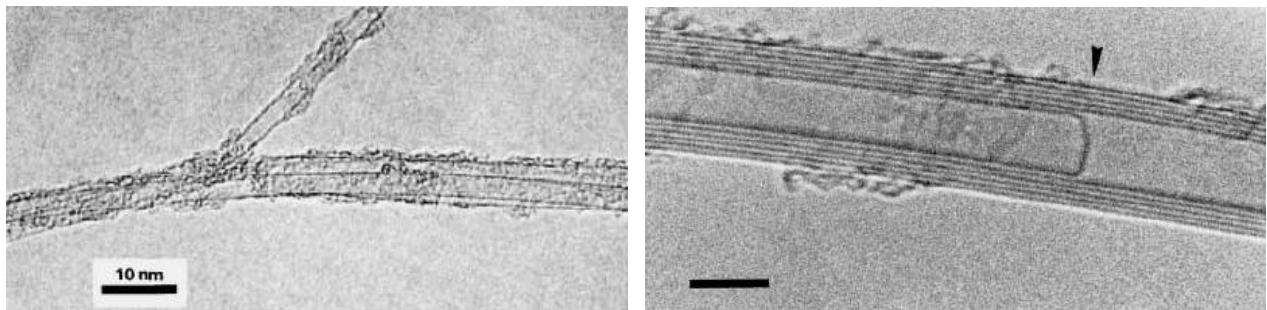
2.3.1 Carbon nanotubes

The introduction of CNTs to the polymer matrices has been a topic much research interest [65, 8]. The availability of low cost fabrication processes and versatility of CNT properties have made them an especially popular composite system to characterize and study for unique applications. Mechanical performance with CNT dispersion at low weight fractions (.25

wt%) have shown to increase mechanical strength and modulus of epoxy systems by 24% and 20%, respectively [7, 8].

Mention of the formation of carbon tubules can go back to the 19th century in a patent for light bulb filaments by Thomas Edison [66]. The earliest evidence of a tubular carbon nanostructure was shown in a 1952 paper [66, 67]. Experiments by the Kroto and Smalley et al. [68] showed the existence of C₆₀ in a unique structure but on a small scale. Iijima (1991) was the first to officially demonstrate the existence of nested carbon tubules (MWCNT), thus, commonly accredited with the discovery of CNTs [66, 69].

Carbon nano-tubes are hollow cylinders of the graphite sheets [70]. Their structure can often lead them to be considered as molecules or pseudo-one dimensional crystals. Typically, CNTs have a high aspect ratio, in that the proportion of its diameter to its length is several of orders in magnitude different; diameters are usually nanometers and lengths in microns. Multi-walled carbon-nanotube tubes can often be made up of several nested, concentric tubes, as opposed to single walled carbon nanotubes (SWCNT) which consist of only single (or sometimes two) cylinder of graphene. Figure 2-14 shows a SWCNT and MWCNT imaged under transverse transmission electron microscope.



(a)

(b)

Figure 2-14 a) Single walled CNT imaged with TEM b) Multi-walled CNT imaged by TEM, scale bar of 5nm.

As shown in Ref [68]

The carbon-carbon covalent bond is known to be the strongest bond found in nature, which is why MWCNT exhibit superior mechanical resistance and are about one sixth the density of steel [65, 71]. Depending on the fabrication method and whether they are in multi-walled or single-walled configurations, CNTs have been measured to have tensile strengths of up to 63 GPa and 54 GPa, respectively [8]. In similar experiments, Young's modulus have been reported to be as high as 1.47 TPa for SWCNTs and 1.18 for MWCNTs. This is far superior to that of commercial carbon fiber which is typically 200 – 350 GPa [8].

2.3.2 Carbon Nanofibers

Carbon nanofibers (CNF) are very similar in a lot of ways to CNTs. However, they differ by their intrinsic structure. CNTs are composed of graphene sheets rolled up into concentric cylinders, while CNFs can be found in two configurations: stacked and herringbone. A stacked configuration consists of multiple sheets of graphene sequentially laid on one another, forming a solid structure. A herringbone configuration is comprised of truncated conicals of graphene stacked on one another; having a hollow core. They usually differ in diameter from CNTs by one or two orders of magnitude. Their structure and size make them approximations of smaller scale, traditional carbon fiber [72, 73, 74]. Figure 2-15 shows common carbon nanostructures in scaled chronology.

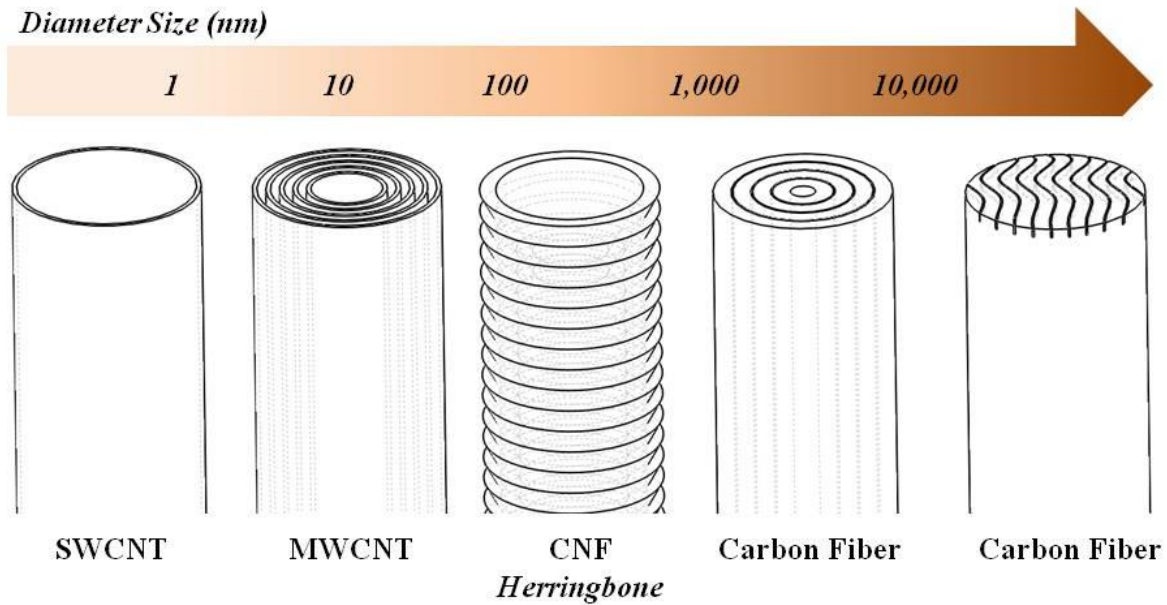


Figure 2-15 Comparison of different carbon tubules structures, modified from Ref. [74].

2.3.3 Polymer Carrier

A “polymer carrier” is used to describe a low viscosity polymer matrix ($< \sim 5000$ cps) that is meant as a transportation medium for particulates order of magnitude larger than the polymer molecules. This technique is often used when a certain substance is not capable of exhibiting fluid like characteristics on its own, at room temperature. As mentioned in section 2.5, direct write technologies require that the materials they process demonstrate rheological properties of fluid so that the system can accurately process it. The myriad of different polymers that are commercially available makes them an excellent option for multiple processing methods. Often times a carrier is selected not just because of its specific rheological properties and compatibility with the constituents of interest, but for its ability to be removed in a post processing step. This is most evident in applications for electronics printings with direct write techniques where the

presence of the polymer component of a conductive ink produces parasitic losses and performance is optimized by its removal [44].

2.3.4 Nano-Composites Research in AM

Promising results from current nanocomposites research in matrix reinforced nanocomposites have utilized common polymer matrices used in additive manufacturing technologies. The proliferation of AM technologies can further the democratization of the manufacturing capabilities of the nanocomposite materials. Improvement of commercial polymeric materials that are available for AM technologies will also extend the reach of their applications and further allow designer to uniquely tailor the properties of the their part.

Research in composite materials for FDM systems have provided insight to some the challenges and potential application of reinforced systems. The introduction of chopped glass fibers into a acrylonitrile-butadiene-styrene (ABS) matrix was success in showing an improvement in tensile strength by 60% at a 18% loading by weight [75]. However, the material was made drastically brittle and difficult to maintain in a continuous filament; a requirement for reliably manufacturing parts with FDM. A similar approach was done with vapor grown carbon fibers (VGCF), which are a larger version of CNTs, known to have similar mechanical benefits. VCGF compositions of 10% by weight within an ABS were measured to improve the tensile strength and modulus of the material by 39% and 60%, respectively [76].

Work in nanocomposites reinforcement for SL resins has also produced promising results. An approach to improve the mechanical properties of an epoxy based resin by interrupting a build and embedding nonwoven fiber glass plies into the cured part showed an improvement in tensile strength [77]. Ceramic nano-composite resins have been implemented in

various applications of producing green bodies or pre-fired ceramic parts [39, 78, 79]. Ceramic composite resin systems are now commercially available for the SL systems. These materials offer higher stiffness and have high heat deflection temperatures, extending their functionality outside of model making [80].

The introduction of carbon nanotubes to a commercially available epoxy based resin for SL (DSM Somos™ Watershed™ 11120) technology was demonstrated to improve tensile strength by upwards for 7.5 % at only .1% weight by volume loadings [12, 13]. The resin's critical exposure observed to be altered and empirically found to be changed by ~30% and ~70% for the concentrations of .025% w/v and .1% w/v. Challenges in dispersion were overcome by modifying the SL tool's (3DS 250/50) vat with a circulation system to ensure constant mixing. A part (chess rook) was manufactured to prove that the material was indeed reliable enough to produce fully complex geometry.

CHAPTER 3 EXPERIMENTAL SETUP AND METHODOLOGIES

3.1 INTRODUCTION

As mention in chapter 2, Direct Print Additive Manufacturing, or DPAM, is referred to as a direct-write technology that has been adapted for constructing macroscale parts. The focus of this study is to develop a DPAM process for constructing parts with a commercially available, Stereolithography resin that has been loaded with carbon nanotubes. To execute the construction with this nanocomposite system, the dispense parameters of the extrusion system must adjusted to optimize the features of the extrusion features for reliable deposition. An intermediate process routine needs to be incorporated between the depositions of each layer so that polymerization of the epoxy carrier takes place. As will be described, a system to ensure accurate alignment between the deposition and curing stages must also be in place so that material deposition is accurately placed. From characterizing the material's response to control and processing parameters, CAD renditions of the final parts can be discerned and digital files can be created to execute construction.

The focus of this chapter is to describe the experimental setup and methods used throughout this study. The materials characterized in this study are introduced. Then a detailed description of dispensing systems is provided, with a full depiction of what is known as the dispense parameters and their impact to the deposition process. A description of the UV curing system used in the study is then provided. Finally, a methodology for the three-dimensional construction of the mechanical test specimen is shown.

3.2 NANOCOMPOSITE MATERIAL

3.2.1 Polymer Carrier

A commercially available resin system designed for the stereolithography system was chosen as the carrier for this project. Somos® Watershed™ XC 11122 by the DSM Corporation [80] is an epoxy based system that polymerizes through a cationic process. Stereolithography resins were chosen for this study because they can be readily solidified with the seamless integration of a UV radiation source. They also are of ultra low viscosity, allowing for higher ratios of nanostructure loading. A carrier with higher viscosity, when aggregated with the same concentrations, would potentially require a pressure to extrude that exceeds what is available from the dispensing system. Table 3-1 list selected properties of Watershed™ XC 11122 as provided by Ref. [81].

Table 3-1 Material properties of DSM Somos® Watershed™ XC 11122, adopted from Ref. [81]

Liquid Properties		Optical Properties		
Appearance	Optically clear	E_C	11.5	mJ/cm ²
Viscosity	~260 cps @ 30°C	D_P	6.5	mils
Density	54 ~1.12 g/cm ³ @ 25°C	E_{10}	54	mJ/cm ²
Mechanical Properties				
Tensile Strength at Break	47.1 – 53.6	MPa		
Elongation at Break	11 – 20%			
Elongation at Yield	3%			
Modulus of Elasticity	2,650 – 2,880	MPa		
Flexural Strength	63.1 – 74.2	MPa		
Flexural Modulus	2,040 – 2,370	MPa		
Thermal Properties				
C.T.E. -40°C – 0°C	66 – 67	μm/m °C		
C.T.E. 0°C – 50°C	90 – 96	μm/m °C		
C.T.E. 50°C – 100°C	170 – 189	μm/m °C		
Electrical Properties				
ϵ_r @ 60 Hz	3.9 – 4.1			
ϵ_r @ 1 kHz	3.7 – 3.9			
ϵ_r @ 1 MHz	3.4 – 3.5			
Dielectric Strength	15.2 – 16.3	KV / mm		

3.2.2 Carbon Nano-Tubes

Two different carbon nanostructures were implemented in this project:

1. Nanocyl™ NC 7000; Nanocyl™ (Sambreville, Belgium)
2. Pyrograf®-III PR – 24 – XT – HHT; Pyrograf Prodcuts Inc. (Cedarville, Ohio)

Nanocyl™ produces a myriad of CNT reinforced products for applications stemming from conductive adhesives to flame barrier coatings to anti-static materials [82]. At the foundation of these products is NC 7000, an industrial grade multi walled carbon nanotube that is produced through a Chemical Vapor Deposition (CVD) process and is available for purchase in bulk form. The average overall diameter of the MWCNT 9.5nm and the average length is 1.5µm. Resulting in an aspect ratio of roughly 158:1. The carbon purity is measured to be 90%, while the other 10% is found in metal oxides. Their surface area has been measured to be between 250 and 300 m²/g. A layer of pyrolytically deposited carbon exists on the surface of the MWCNTs [83].

Pyrograf Products Inc. focuses on the production carbon nanofiber structures that are very fine, highly graphitic (planar carbon structure), and low cost [84]. Of the two CNFs offered by Pyrograf, the PR – 24, XT – HHT grade was chosen. The PR – 24 type CNF has an average diameter of 100nm and is produced through a chemical vapor deposition process. The XT designation indicates that the vapor grown fibers were run through a debulking process to achieve a uniform bulk density (~1-3 lb/ft³). The HHT abbreviation indicates that the fiber was heated treated to 3000°C to produce a fully graphitized fiber form, also reducing the iron content to very low levels (< 100 ppm) [84]. The bulk CNF products has a surface area of 41 m²/g. Fiber lengths are estimated to be between 50 to 200µm, resulting in aspect ratios between 500:1 and 2000:1.

3.2.3 Material Mixing

The carbon nanostructures were combined with the polymer carrier in three different concentrations. All concentration measurements are denoted by the percentage of the weight represented by the solute (carbon nanostructures) within a given volume of the solution (polymer carrier). The concentration percentage is read as “percent weight by volume”. The formulation is for the material designation is depicted in Equation (3-1).

$$\% (w/v) = \frac{\text{weight of solute (g)}}{\text{volume of solution (mL)}} \times 100\% \quad (3-1)$$

The density of the polymer carrier is indicated in Table 3-1 as 1.12 g/cm³ (cm³ = mL). Therefore, this representation of the nanocomposite’s concentration can be approximately interpreted as the weight composition of carbon nanostructures within the nanocomposite. The different nanocomposite concentrations used in this study are shown in Table 3-2. Viscosities of the material concentrations were not experimentally quantified. Distinction between the viscous consistencies amongst the concentrations was noted and labeled in Table 3-2. The low end represents a similar viscosity to hair gel, while the high end draws similarities to clay.

Table 3-2 Nanocomposite concentrations given as percentage of solute weight by volume.

Carbon Structure	Concentrations		
Nanocyl™ NC 7000	1 % (w/v)	2.5 % (w/v)	5 % (w/v)
Pyrograf®-III PR – 24 – XT – HHT	5 % (w/v)	10 % (w/v)*	
	<i>low</i>		<i>high</i>

A preliminary test for dispense feasibility was performed with each of the concentrations to determine whether the systems was capable of extruding the material. The 10 % (w/v) concentration was observed to be “indispensable” for the pressure required to displace the

material within the dispensing system exceed the machine specification. Therefore this material concentration was omitted from the study.

The nanocomposites were mixed in a stainless steel two roll mixer until a desired consistency was observed. The 1% (w/v) loading of Nanocyl was mixed for approximately 1 hour while all other concentrations were mixed for half an hour. To avoid premature polymerization, the materials were all mixed in darkened ambient lighting and stored in opaque containers.

3.2.3.1 Material Loading

The deposition system used in this project (see 3.3) requires that the material of interest is loaded in a syringe that is back-sealed with a piston cap. For long run applications (i.e. entire syringe reservoir is used), it is paramount that pockets of air (air bubbles) are removed from the material reservoir. Air bubbles will introduce discontinuities in material flow that form parasitic pores in the structure. A material layer with voids will prevent reliable and uniform deposition of the subsequent layer. They also have the potential to completely interrupt consistent flow and skew the extruded features.

The nanocomposite material concentrations were first put into a standard laboratory beaker (cleaned with acetone and let dry at room temperature) and vigorously stirred by hand for roughly 3 minutes. This helps remove some air bubbles trapped in the bulk material. Then the materials were loaded into a sacrificial syringe through the large orifice with a standard laboratory spatula. Once the desired amount of material was in the sacrificial syringe, it was pushed through, to the small orifice and through a luer – to – luer adapter. The syringe reservoir that would eventually get mounted to the dispensing system was then attached to the material

loaded syringe (sacrificial syringe) and the material would be manually transferred. Figure 3-1 shows the syringe loading apparatuses described. Black electrical tape (not shown in Figure 3-1) was wrapped around the syringe reservoir to eliminate the material's exposure to ambient lighting.

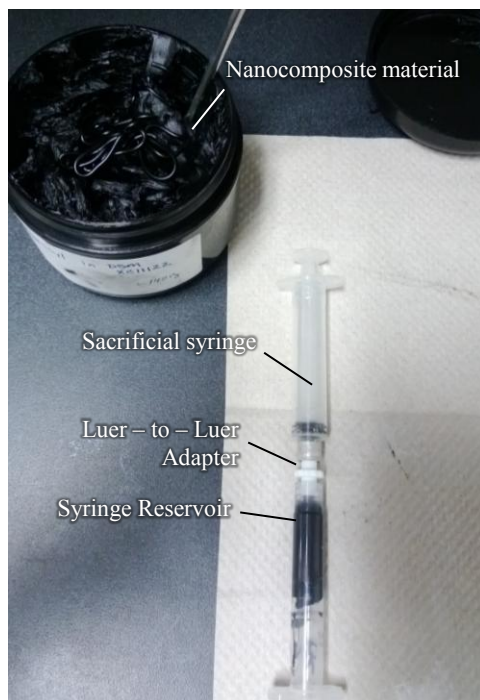


Figure 3-1 Components used to loaded syringe.

3.3 DPAM SYSTEM DESCRIPTION

3.3.1 nScript System Overview

The formation of nScript has its roots in DARPA's Mesoscopic Integrated Conformal Electronics (MICE) program which started in 1999. This multi-million dollar program was set in place for the advancement of direct-write technologies and materials for electronics fabrication on virtually any surface. The nScript technology was designed and developed by Sciperio

(Orlando, FL) as an answer to the call from DARPA MICE and then was spun off into its own company in 2002.

The nScript SmartPump™ is an nozzle extrusion based system that is capable of depositing materials that exhibit viscosities from 1 cps (e.g. water) to 10^6 cps (e.g. clay putty) [50]. This makes it well suited for 3D deposition applications where the higher the viscosity a material is, the better suited it is for 3D fabrication (see 2.2.5.3). The pump is capable of controlling volumes down to 20 pL and offer a 100 pL pump as well. The gantry system which the pump is mounted on, allows has $\pm 5\mu\text{m}$ resolution and an X/Y motion repeatability of $\pm 2\mu\text{m}$; $\pm 1\mu\text{m}$ in the Z direction. Retrofitted on the system is a Z-mapping sensor that takes a scan of the substrate's topology. This map is incorporated into the pump's motion path to accurately ($\pm 12\mu\text{m}$) maintain the pen tip's (extrusion nozzle) distance from the substrate consistent. Typical build substrates (as implemented in this project) are performed on a Kapton® film that is mounted on the nScript system's build platform. The build platform used is a ground flat porous aluminum vacuum chuck that is 300mm by 150mm by 100mm. A position – adjustable camera is mounted to the side of the dispense mechanism and is focused on the pen tip. This provides the system operator with a real time video stream of the deposition process. A typical printing set up is shown in Figure 3-2.

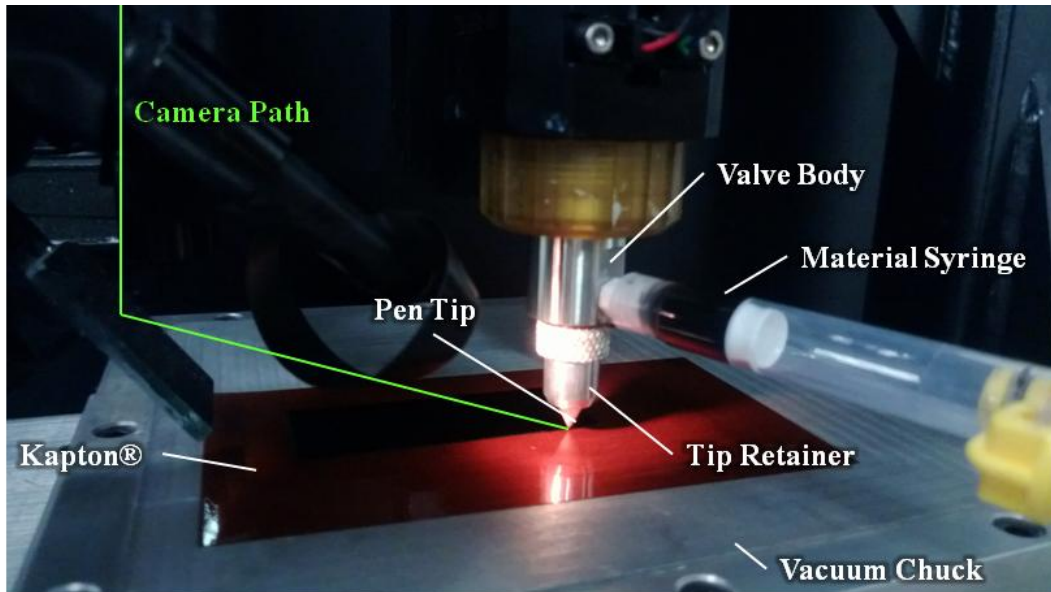


Figure 3-2 Typical nScript deposition system configuration.

3.3.1.1 Dispense Mechanics

The SmartPump™ system consists of the several mechanical parts that physically interact with the material to achieve extrusion control; these are called hardware parameters. The motion (i.e. speed, displacement) and size of these parameters, along with the gantry motion, are what impact the repeatability and feature size of the extruded material. Figure 3-3 shows cross-sectional representation (not drawn to scale) of the nScript SmartPump™ system.

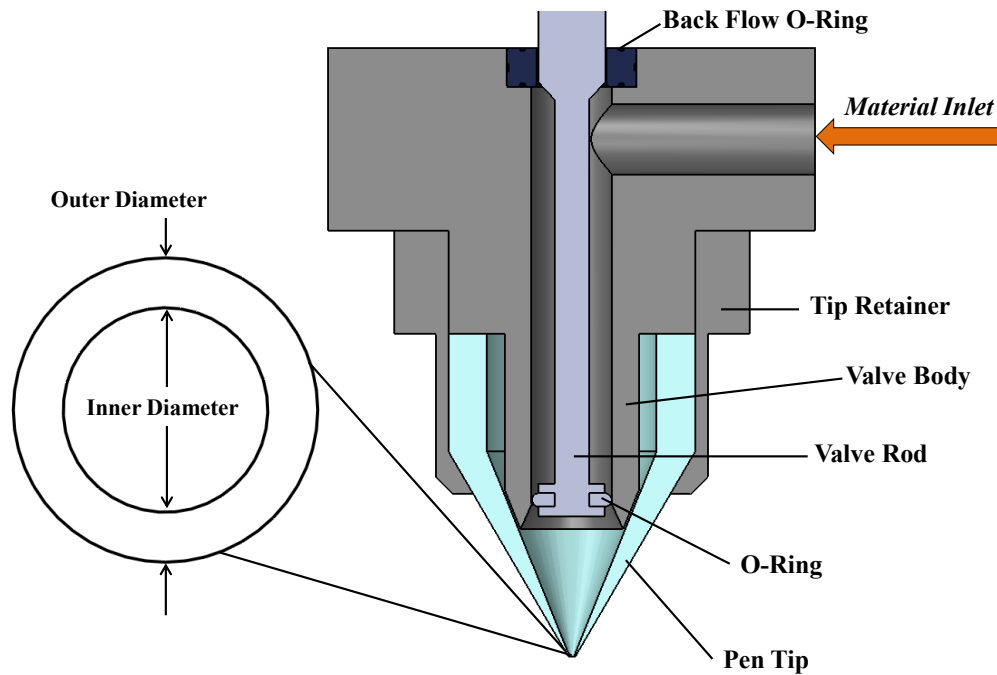


Figure 3-3 SmartPump™ hardware schematic

Material flows into the pump system through an inlet in the valve body; as shown in Figure 3-3. A variable pressure air source (0 to 100 psi) provides a constant, quasi – static force to the syringe reservoir. The term quasi – static is used because the amount of time necessary for the force, acting on the material, to change is orders of magnitude less (seconds) than the rate of deposition and the response of the other control parameters (microseconds); even for low viscosity materials that exhibit a low resistance.

As the material flows through valve body, it comes in contact with the valve rod. Flow is restricted in the upwards direction (in reference to Figure 3-3) by an o-ring and is force downward, along the valve rod. At the valve body's outlet a seal is formed between an o-ring, attached to the end of the valve rod, and chamfered edge of the valve body. The valve rod can then be displaced with $\pm 1\mu\text{m}$ of accuracy to release material and allow it to make its way out of the pen tip's orifice. The pen tip's conical design inhibits parasitic pressure drops which may clog

the material within the tip. The enclosed volume within the pen tip also experiences an aspirating function as the valve rod is retracted into the valve body [56]. This provides further control at the incipient (start) and terminal (stop) material deposition points.

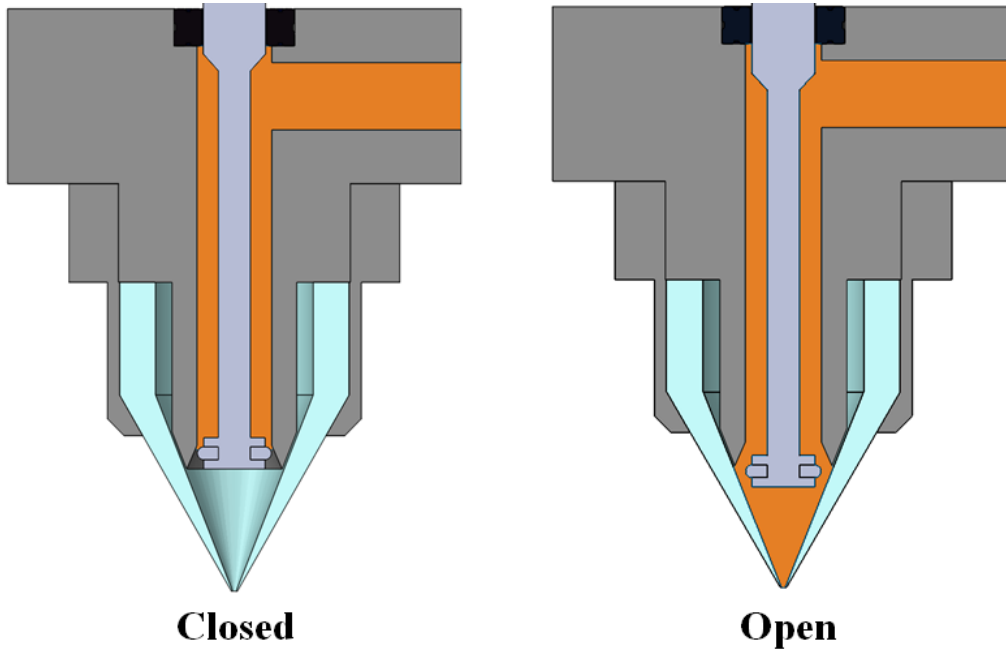


Figure 3-4 Open and closing mechanism for the nScript SmartPump™

3.3.1.2 Dispense Parameter Description

The nScript system has several dispense settings that can be adjusted to achieve particular feature size of deposited lines. The characterization of the material's response to these parameters is essential in being able to achieve a repeatable process. Table lists the parameters that are adjustable within the system.

Table 3-3 List of system control parameters.

Parameter	Description
Dispense Gap	Distance from pen tip orifice from substrate. (μm)
Back Pressure	System regulated pressure applied to syringe reservoir. (psi)

Print Speed	Rate at which entire extrusion system is displaced.	(mm/s)
Valve Opening	Distance valve rod is displaced.	(mm)
Valve Speed	Rate at which valve rod is displaced.	(mm/s)
Dwell Time	Amount of time the system is motionless with the valve open.	(s)
Pen Tip Inner Diameter	Orifice diameter; through which material is extruded.	(μm)
Pen Tip Outer Diameter	Diameter of pen tip's outer edge.	(μm)

Compounding effects are observed when adjusting these parameters to achieve desired results. Daraj [85] showed through an empirical regression analysis that material viscosity, dispense gap, and back pressure can have an impact on the height of the material. In the same study it was also shown that the interaction between pressure and dispense gap influences the other in with width of the lines that can be achieved.

An optimal line feature is achieved such that the dispensed line width does not exceed the pen tip's outer diameter, the line thickness matches the dispense gap, and the line remains continuous. For extruded material to adhere to the substrate, the materials surface energy to the pen tip (ceramic) must be overcome in a controlled manner. Therefore, a narrowed tolerance dispense gap must be maintained. It is necessary for the material to make enough contact with the substrate that the superposition of the substrate's surface energy with the material and the back pressure forces overcome the desire for material to stick to the pen tip. In some applications, with unique materials, it is possible to produce line features that are of the width of the inner diameter [58]. This requires materials that are high in viscosity ($< 200,000$ cps) and demonstrate unique rheological properties and surface chemistries with the substrate.

Ideally, the print speed should be similar to the material's exit flow rate (speed at which material is being extruded) to the desired feature size. If the extrusion system is moving much faster than the material's flow rate, not enough material will be deposited at desired locations and vice versa. Flow rate is primarily and typically controlled by the back pressure and pen tip dimensions. Li et al. showed that flow rate is also impacted by the dispense height, concluding that pressure is dominated by the substrate at smaller dispense gaps and a transient region exists as pen tip is moved further [56].

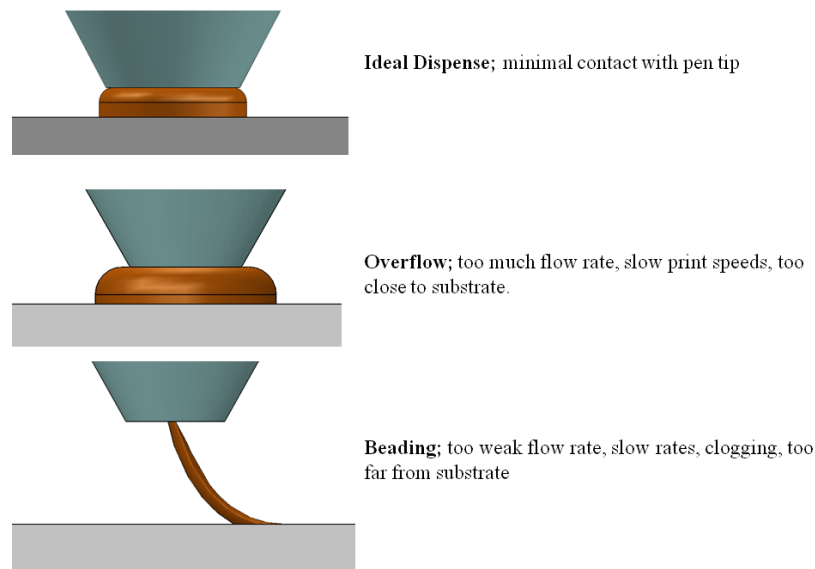


Figure 3-5 Illustration of dispense common dispense scenarios, modified from [85].

3.3.2 Ultra – Violet Curing Apparatus

The ultra – violet radiation source used was a Porta Cure (PC) 1000F unit from American Ultraviolet (Lebanon, IN) [86]. The unit consisted of a radiation source (bulb) and power control box. The bulb at its highest setting is rated at 400 W/in; the control box could be set to three settings. It should be noted that this rating represents that amount of electrical (not irradiance) power delivered to the bulb per unit length of the bulb (e.g. a 10” at 400 W/in has 4000 W

applied to it) [87]. The mercury vapor bulb in the PC 1000F emitted a omni-chromatic UV spectrum; the relative intensities are shown in Figure 3-6. The bulb apparatus was positioned on top of two 4 inch, aluminum, 80/20 beams, putting the samples within the cure arc.

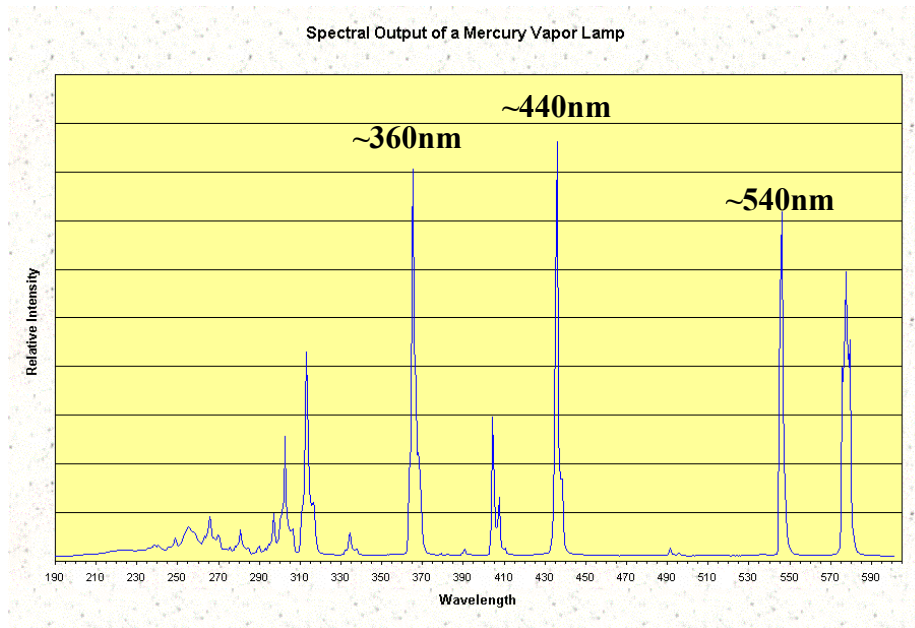


Figure 3-6 Relative intensities of the PC 1000F bulb across UV spectrum (courtesy of American Ultraviolet)

Initial tests of the nanocomposite material under UV radiation at each of the three setting showed that the material could not withstand prolonged exposure (seconds) at neither the ‘high’ nor ‘mid’ setting. The preliminary test would begin to curl and delaminate from the Kapton® substrate; visible out gassing (i.e. smoke) would be visible. Figure 3-7 shows the results of material under prolonged exposure. Only the ‘low’ setting was observed to not cause any of the material concentration samples to not delaminate. Thus, it was chosen as the constant level for all the curing samples.

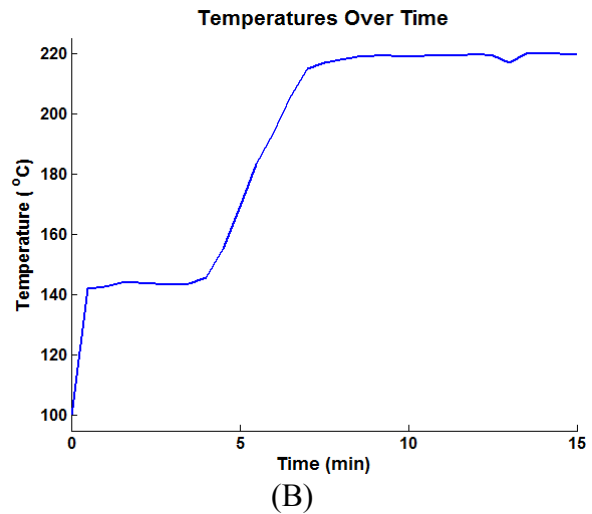


Figure 3-7 Nanocyl 1% (w/v) after ~5 seconds of the exposure at 400 W/in².

The mercury vapor bulb experienced a transient state upon turning on. Finding the when the bulb reached steady state in power output is critical for achieving repeatable curing results. A temperature quantification of the radiation platform was done to elucidate how long it would take for the bulb to reach steady state. The temperature was monitored with a CT – M3 bolometer from Micro – Epsilon (Raleigh, NC) [88]. The working distance was set to 13 inches, which gave it a 7 mm spot size [89]. The control box Temperature values from the bolometer’s control box were recorded every 30 seconds and the process was truncated once six steady state values were recorded. The results are shown in Figure 3-8. The temperature readings indicate that the mercury bulb takes approximately 7 minutes to reach a steady state energy output; base of the temperature readings. Therefore, the bulb must be left on and not switched intermittently during the printing process. A shutter mechanism is needed to contain hazardous scattering and consistent exposure in between layer depositions.



(A)



(B)

Figure 3-8 (A) Temperature measurement set up (B) Temperature variations of cure stage on 'low' setting.

3.3.3 DPAM Printing Procedure

The part fabrication procedure is illustrated in Figure 3-9. Before starting a print routine the origin of the part must be set. This is the X and Y coordinates from which the extrusion is relatively motioned. This ensures that this location maintained for the deposition of each layer. Once a layer is fully deposited, the build substrate is removed from the nScript dispensing system and is transitioned to the UV curing apparatus. It is imperative that the extracted, unfinished part gets insert back onto the build platform accurately. This alignment procedure was accomplished in three steps on the nScript build platform. First, an accurately cut, straight edge Kapton® substrate was cut with a conventional paper cutting tool. Second, the top edge of the Kapton® was pushed to meet a wall created by a flat aluminum block at the top of the build platform. This process was then repeated at the rightmost edge. Finally, the vacuum chuck was activated, securing the Kapton® substrate in place.

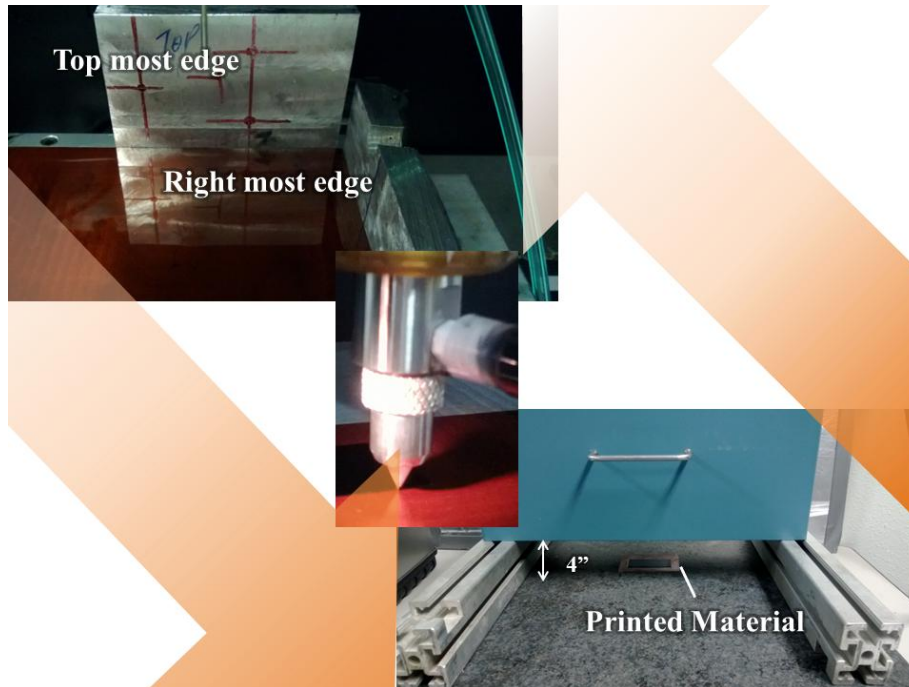


Figure 3-9 DPAM process station; (A) UV curing apparatus (B) nScript build platform

Between every layer the dispense gap must be found with the pen tip. This is done by moving the pen tip over to the predetermined origin (location where print starts). The pen tip is then brought down to the surface of the substrate layer until it is observed in the process view camera to touch the surface of the material. The Z position is registered then the pen tip is readjusted to the desired dispense gap.

The topology of the build platform which the materials is dispensed onto is of the utmost importance to the reliability of the platform. The nScript system's Z – scanning capability is an enabling feature to correct inconsistencies in the leveling of the platform. However, a more robust approach is to ensure the system hardware is within certain tolerances. The Z – scanning sensor was used to scan the vacuum chuck (build platform) and a three dimensional point cloud was generated. The point cloud data was then input into MATLAB® and visualized; this is shown in Figure 3-10. The figure illustrates that there is some fluctuation on the platform but does not exceed changes over $\sim 3\mu\text{m}$, which is flat relative to this application.

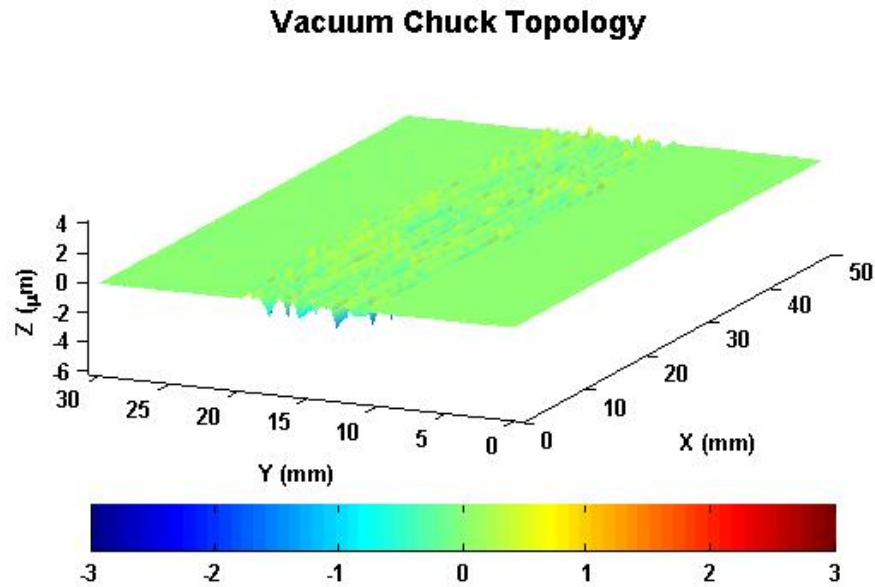


Figure 3-10 Topological scan visualization of the vacuum chuck area where parts were built

3.4 SPECIMEN BUILD STRATEGY

3.4.1 Part Construction Methodology

The dimensions of a single line dispensed with a given set of parameters must be characterized then used to create a CAD model. A series of lines will be printed under certain set of process parameters. The widths and thicknesses will be measured with an optical microscope to measure the width and then a scanning electron microscope to determine the thickness. The list of parameters setting is show in Table 3-4. The parameters were found by observing several conditions to which the material would produce consistent and repeatable flow. The pen tip used in this study is shown in Figure 3-11 ; the image taken and measured under an optical microscope A series of lines at these settings were dispensed at three different dispense gap and the width were measured.

Table 3-4 List of print parameters settings used to dispense the line characterizations

Variable	Value	Units
Print Speed (90°)	70	mm/s
Print Speed (0°)	50	mm/s
Valve Speed	8	mm/s
Valve Opening	.3	Mm
Valve Wait	.01	Seconds
Pressure	20	psi

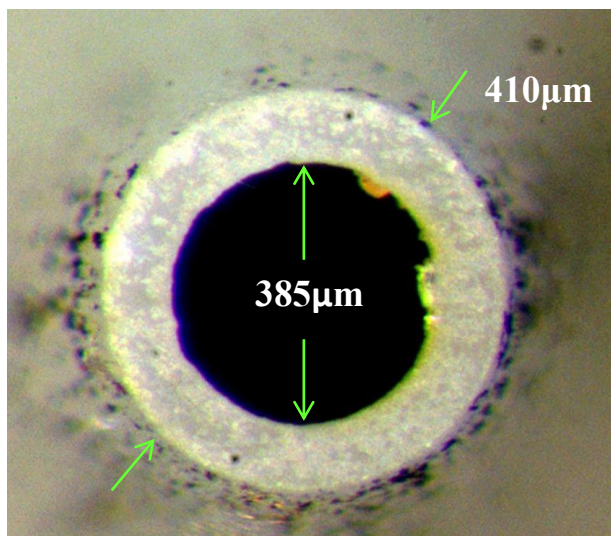


Figure 3-11 Pen tip dimensions used throughout study

3.4.2 CAD Design

The design for the mechanical test specimen is shown in Figure 3-12. The specimen layers are designed in the nScript proprietary software, PCAD. This software allows for the user to make two dimensional, scaled drafts of the pump's motion path. Actual line dimensions are not predetermined in the software and must be accounted for by the user based on empirical measurements. Fill patterns are performed in a serpentine pattern. This means material is continuously extruded from the beginning of the layer to the end so that is the edges of the layer are composed of short line segments in the direction of the pitch translation. At the turns of the

serpentine pattern the motion control negatively accelerates the extrusion head and then positively accelerates it to meet the set print speed. This inconsistency in speed leads to a non-uniform volume of material the edge. The direction layers are dispensed were designed to be orthogonal to one another. This ensures that the contact between subsequent layers is made. The 90 degree orientation signifies the direction along the short dimension (width) of the part, while the 0 degree orientation is along the long dimension (length).

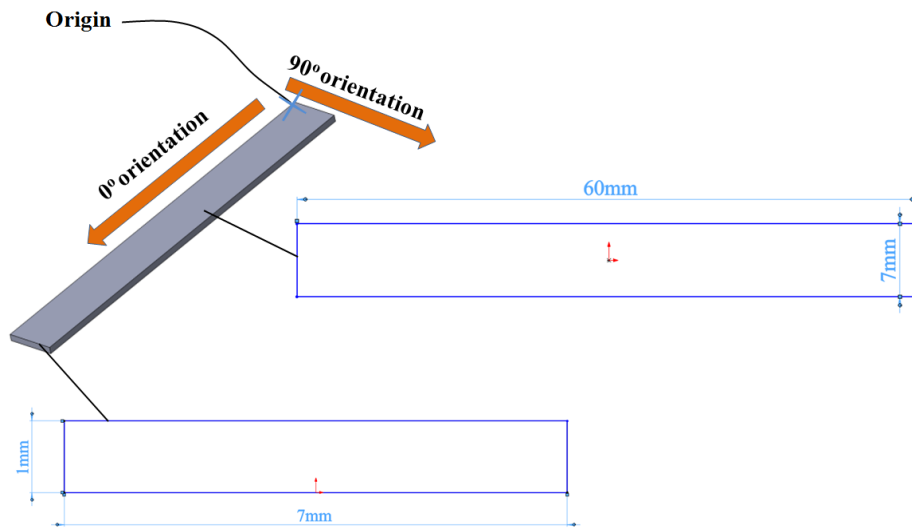


Figure 3-12 (A) Design mechanical test specimen (B) 90 degree orientation (C) 0 degree orientation

The spacing between lines is known as the pitch. This is usually set to be the width of the line, which is tuned to match the pen's tip outer diameter (see Figure 3-5) By doing so, lines will theoretically be adjacent to one another. However, this is not realistic. Inconsistencies in the material, ambient conditions, and equipment can cause the material to behave irregularly during the printing process. A statistical analysis of line variability can help account for this but it is good practice to the employ an overlap when designing the fill pattern, as shown in Figure 3-13. Also, the realistic profile of a line is elliptical and not square. Even assuming small variations in line widths, dispensing directly next to lines will cause the layer to have an undulated surface;

unwanted in the printing process. An overlap is essentially a percentage of the line width that is reduced to the pitch such that the lines run into each other; is defined by Equation (3-2).

$$\text{pitch} = (\text{line width}) - (\text{line width} \times \text{overlap}) \quad (3-2)$$

It should be noted that the overlap parameter is can have negative effects on the printed parts. Lines that overlap too much will cause excess material accumulation on the pen tip. This causes the surface of a layer to become uneven and potentially causing the same effects as air bubbles (see 3.2.3.1). Therefore, this parameter should be statistically quantified or modeled to best optimizes builds.

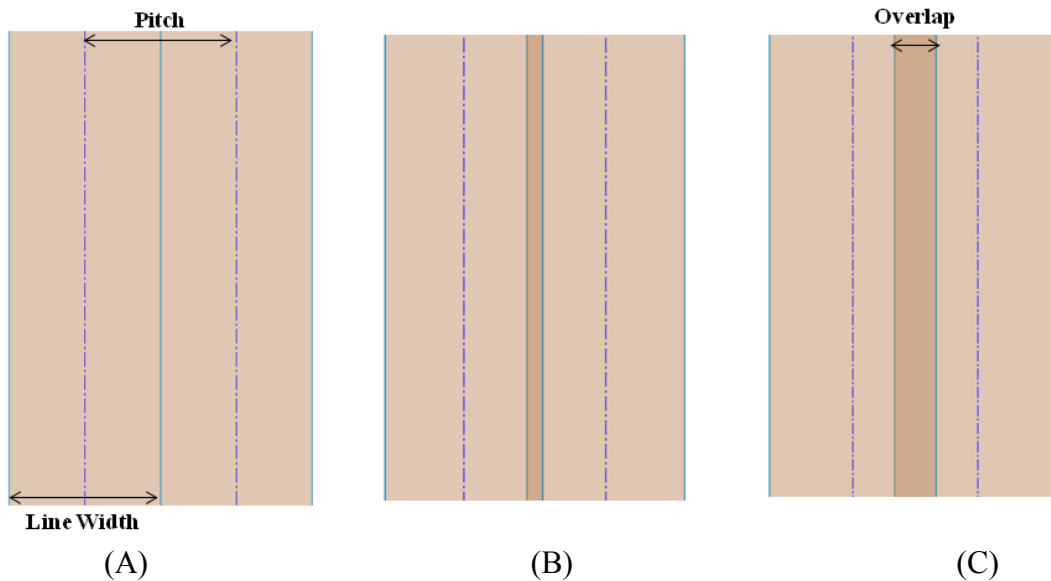


Figure 3-13 (A) Overlap = 0 (B) Overlap = .1 (C) Overlap = .25

CHAPTER 4 EXPERIMENTAL RESULTS AND OBSERVATIONS

4.1 SPECIMEN CONSTRUCTION

4.1.1 Line Width Measurements

A study of the effects of the dispense gap was performed on each of the material concentrations, while all other parameters were held constant. This was done to quantify the impact the dispense gap has on the line widths and then measure thickness that is produced. The line width is used to design the fill pattern of each layer. The list of the parameters implemented is shown in Table 3-4.

Each material was dispensed five times at dispense gaps of 50 μ m, 70 μ m, and 100 μ m. A coarse resolution of the dispense gap values was used because a general trend is only necessary to quantify how the material behaves under these conditions. The lines were dispensed sequentially and then simultaneously cured under the mercury bulb for ~10s at the lowest power setting (150 W/in). The cured lines were then measured with an optical microscope at 6.3X zoom. The recorded values for each material, at each dispense gap level, was averaged to distinguish a trend. Figure 4-1 shows the plotted averages of the measured line widths versus the different dispense gap measurements. The dashed lines indicate the average line widths over three dispense gaps. The raw data from the experiments can be found in **Error! Reference source not found.**

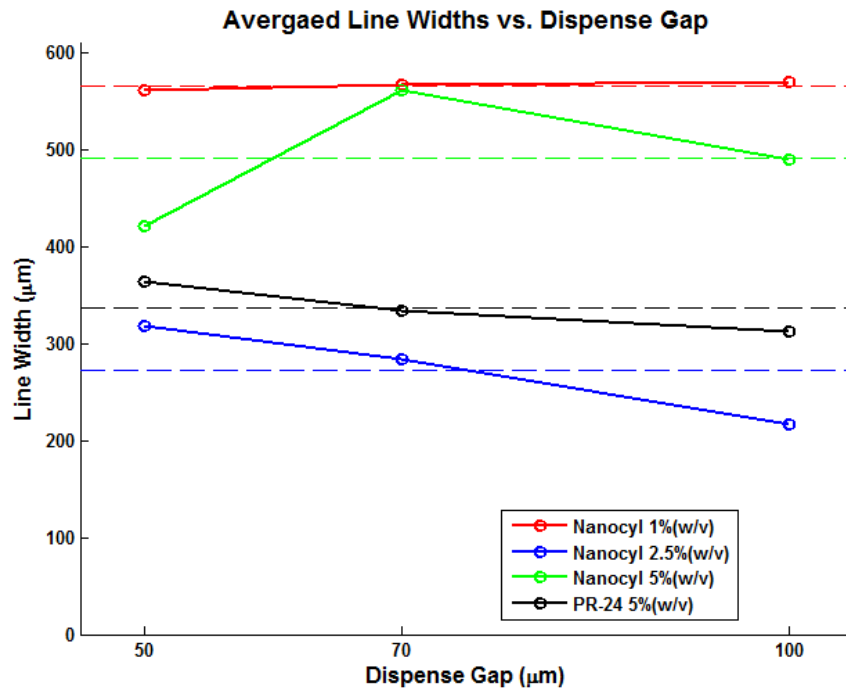


Figure 4-1 Plot of averaged line widths vs. dispense gap.

The Nanocyl 1% (w/v) material appeared to not exhibit much deviation ($\mu = 567.1\mu\text{m}$, $\sigma = 4\mu\text{m}$) relative to the other materials. This suggests that at this deposition speed (70 mm/s) the flow rate is fast enough and the pen tip dimensions are sufficiently large that the dispense gap does not impact the line dimensions. The material concentrations of Nanocyl 5% (w/v) and PR-24 5% (w/v) exhibit negative trends as the dispense gap was increased, signifying that lines got thinner. The linear appearance of the trend be indicative that the material's cross sectional shape can be controlled by adjusting the dispense gap. The Nanocyl 5% (w/v) appears erratic and it could indicate that at this concentration of Nanocyl CNTs and pressure, the nanocomposite begins to exhibit non-linear rheological properties.

4.1.2 Line Thickness Measurements

The line thickness determines the size of a given layer that can be realized. Lines were dispensed on a Kapton® substrate at a 70 μm dispense gap, with the parameters listed in Table

3-4. The dispensed lines were cured under UV radiation set to the lowest setting (150 W/in²). Once cured the lines were sheared with standard scissors and then imaged with a scanning electron microscope using relatively similar magnification. The results are show in Table 4-1. Based on the thickness values it can be deduced that some slumping did occur for the lines of PR – 24 5% (w/v) and Nanocyl 2.5% (w/v). The case for the other two may be a result of overflow; it cannot be made apparent since the line widths are close to the pen tip’s out dimension (see **Error! Reference source not found.**).

Table 4-1 Thicknesses of lines dispensed at the parameters in Table 3-4 and at a dispense gap of 70µm.

	Nanocyl 1%	Nanocyl 2.5%	Nanocyl 5%	PR - 24 5%
Line Thickness	146.19 µm	47.41 µm	99.73 µm	52.20 µm

4.1.3 Specimen Build Results

The mechanical test specimens were fabricated with a pitch 400µm to match that of the pen tip used. Based off the line dispense gap study the pressure was adjusted such that the material flow would match the pitch width. Print parameter values are provided in 5.2APPENDIX B. The parameters adjusted was for pressure the Nanocyl concentrations of 1% (w/v), 2.5% (w/v), and 5% (w/v) were set to 12 psi, 50 psi, and 20 psi, respectively; the PR-24 5% (w/v) material was set to 50 psi. Exposure was also varied for the material concentrations because of the observational response of the respective material to irradiance. The times used were ~10 seconds, ~5 seconds, ~15 seconds, and ~5 seconds for the Nanocyl 1% (w/v), Nanocyl 2.5% (w/v), Nanocyl 5% (w/v), and PR-24 5% (w/v), respectively. Since part extraction from the cure apparatus was performed manually, approximate cure times were used. The temperature of the surface upon which the material was in the UV curing apparatus was observed in between

each layer. All values were approximately between 222°C and 223°C (see section 3.3.2). The material's surface temperature was not recorded because of the lack of alignment accuracy.

The print direction was transposed with each subsequent layer and the dispense gap was set to 70µm between each layer. This gap was chosen because at low gaps (< 50µm) material flow was observed to be inconsistent (see 3.3.1.2) resulting in faulted lines. At larger gaps (> 100µm) too much material would be deposited and it would absorb too much heat, causing the delaminating effects discussed in 3.3.2. Therefore, a dispense gap was chosen in between these two limits.

Layers were deposited then cured for about, as described in 3.3.3. Between each cured layer the value Z coordinate of the pen tip touching the previously deposited layer was recorded. This process was repeated until the aggregated thickness surpassed one millimeter. Plotted in Figure 4-2 is the thickness for each layer for a specimen. The dashed lines drop down to the corresponding layer for each material. Table 4-2 shows the statistics calculated for the layer thicknesses.

Apparent in Figure 4-2 is that the Nanocyl concentrations of 1% (w/v) and 5% (w/v) fluctuate drastically, as indicated by the sawtooth-like pattern. This indicates that these concentrations are affected by the varying dispense orientations. This could potentially be a result in the intrinsic flaw with serpentine patterns. Likewise, an apparent divergence from the observed characteristics of the other Nanocyl concentrations was also witnessed in the line dispense study; suggesting that there is an interaction with between the CNTs and the polymer carries at these concentrations. Furthermore, the CNF system and the 2.5% (w/v) concentration of Nanocyl produced results that they infer the materials are controllable under these parameters. A sawtooth-like pattern is also present but exhibits much smaller fluctuations; further represented by their standard deviations, 16.62µm (Nanocyl 2.5% (w/v)) and 11.89µm (PR-24

5% (w/v)). This indicates that these two materials may be better suited for an autonomous 3D construction application because of their more repeatable thickness control.

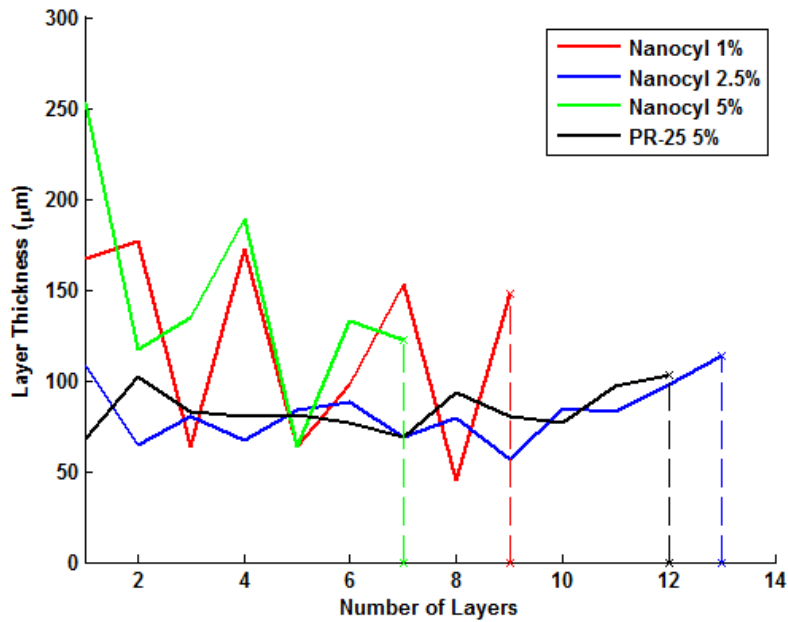


Figure 4-2 Graph of each layer’s thickness

Table 4-2 Statistics for change in layer thickness measurements

	Nanocyl 1%	Nanocyl 2.5%	Nanocyl 5%	PR – 24 5%
Mean	120.89	82.77	144.71	84.17
Standard Deviation	52.93	16.62	60.16	11.89

Imaging of the test specimen under an optical microscope at 1X zoom is shown in Figure 4-3. The Nanocyl concentration of 1% (w/v) is depicted in Figure 4-3 as having a glossy texture. This is undoubtedly a result of the higher content of the polymer matrix present in the bulk. This is witnessed in the width measurements illustrated in Figure 4-3. The designed dimensions this is because the dispense motion path was set at 7mm, where the path is centered to the pen tip meaning an excess of the 600 - 800µm was expected the width and length. The 5% (w/v) concentration of Nanocyl and PR-24 were wider than Therefore, it can be deduced from the

width measurement shown in Figure 4-3. that all the materials experienced some shrinkage while being exposed to the heat generated from the UV curing apparatus

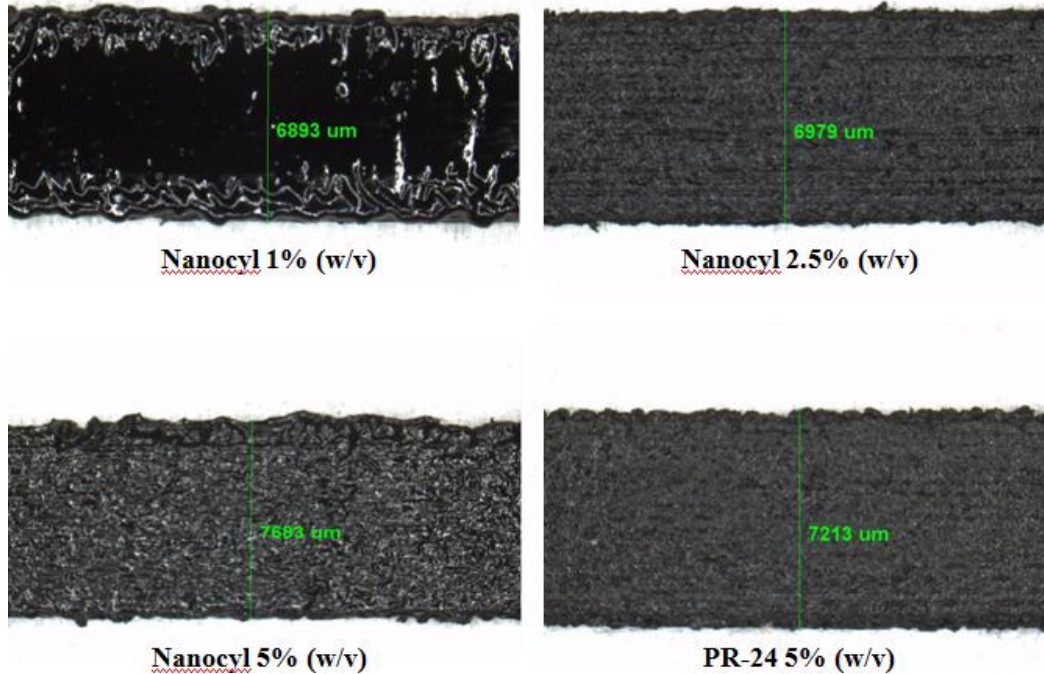


Figure 4-3 Optical imaging of the mechanical test specimen with width measurements

4.2 MECHANICAL EVALUATION

The printed specimen's mechanical characteristics were evaluated until failure (i.e. break) via an INSTRON® 5866 (Norwood, MA) testing apparatus. Mounted on the tool is a calibrated 10 KN load cell and has a $\pm 0.5\%$ accuracy and 0.5% repeatability rating. Diamond serrated gripping faced were used to avoid slippage during the test. The top grip position was adjusted and calibrated such that the specimens were held by 20mm from their length's edge on either side. All tests were conducted at a rate of 5mm/s and were terminated after the specimen was fractured. The data and statistics generated by the INSTRON® experimental software is provided in **Error! Reference source not found.**

An unloaded polymer (DSM Somos™ Watershed 11122) was used as the control data point. It was constructed through a traditional SLA process because the stand-alone polymer's viscosity is too low to be suitable for a DPAM process. Five control specimens were tested; their average tensile strength and Young's modulus were 52.401 MPa and 3.07 TPa, respectively. These values are within 3% (tensile strength) and 8% (Young's modulus) of the values reported by the manufacturer's datasheet [81]. Figure 4-4 shows the stress – strain curve generated by the control specimen.

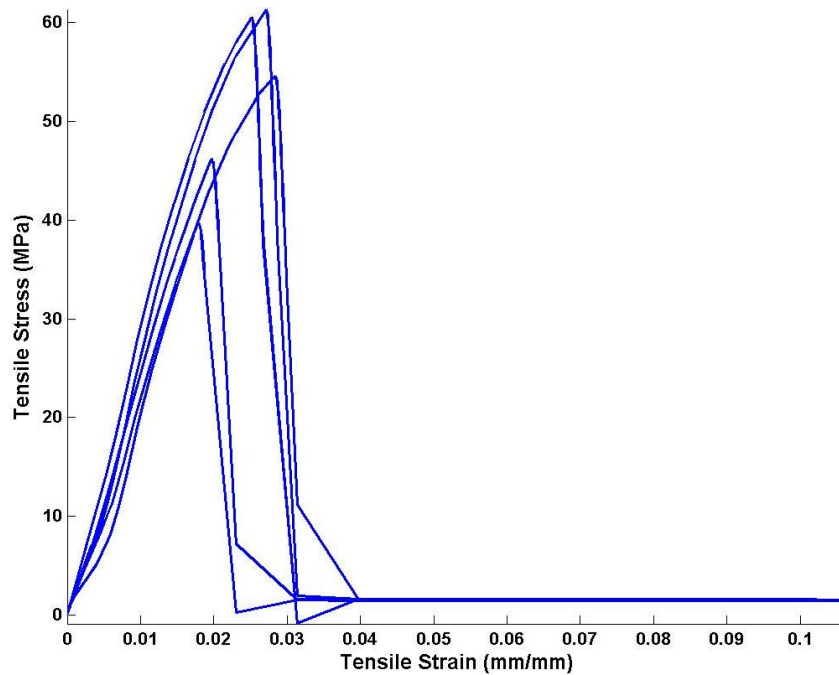


Figure 4-4 Stress-Strain curve generated from the Somos™ Watershed 11122 mechanical evaluations

In Figure 4-5 the average stress – strain responses of the nanocomposite materials is plotted. It is clear from Figure 4-5 that the carbon nanostructures influence the properties of the material. As will be discussed in section 4.3, the introduction of the carbon nanostructures to the material inhibits energy penetration into the structure. The test specimens made up of the nanocomposite material were not representing the bulk properties of fully consolidated material and the characteristics shown were dominated by slipping at the interface of the solid layers and uncured resin with the specimens. Therefore, an inverse relationship between the amount of

carbon nanostructures present within the polymer matrix and the material's mechanical integrity is observed. This relationship is most apparent when the control specimen's stress – strain response is compared with the nanocomposite material concentrations, as provided in Figure 4-6.

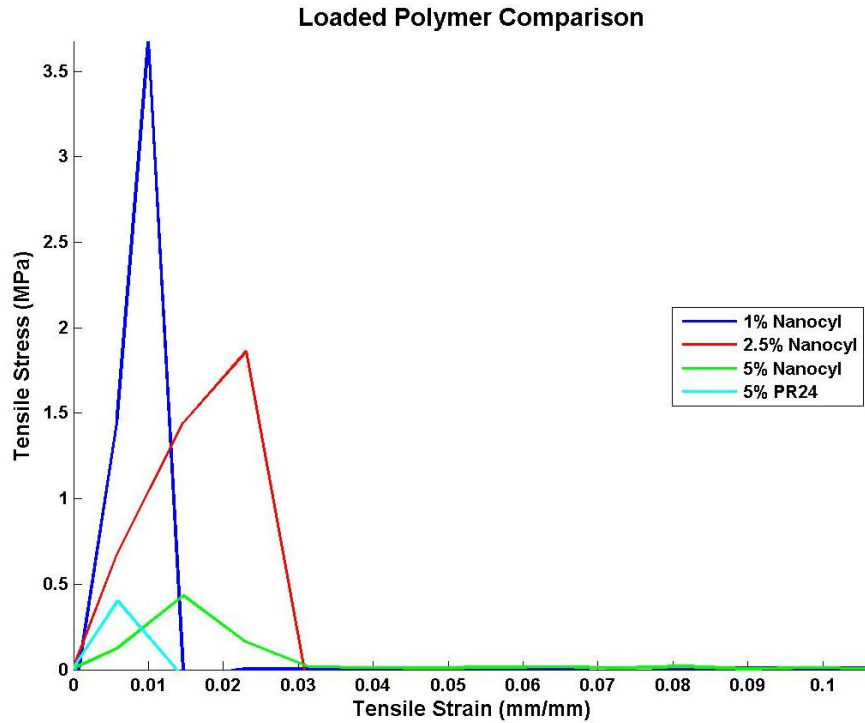


Figure 4-5 Stress-Strain curve generated from the mechanical evaluations of the nanocomposite variations

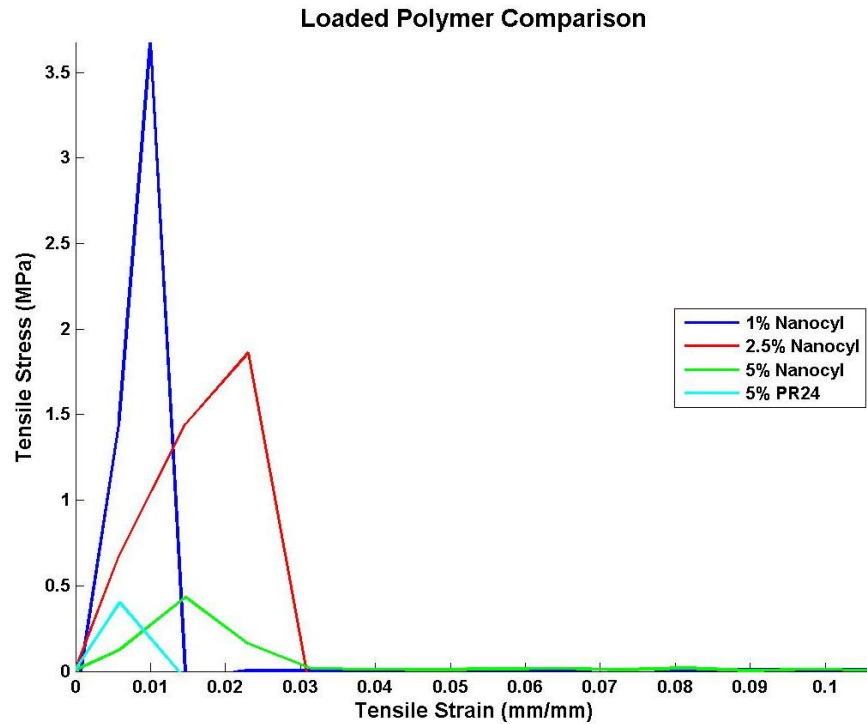


Figure 4-6 Stress – strain comparison between all mechanical specimen.

4.3 FRACTURE IMAGING

All fractured mechanical sample were imaged under a scanning electron microscope to closely observe the interfaces of the layers of the material. As discussed in section 4.2, the mechanical specimens tested were not fully consolidated during the build process. Figure 4-7 show a cross section of a fractured 1% (w/v) Nanocyl meachanical specimen. It is evident that there were layers of uncured resin between the cured layers during the mechanical evaluation. Measurements of the visible layers for the Nanocyl 1% and 2.5% (w/v) specimen showed that the average layers were 51.01 μ m and 39.1 μ m, respectively (5.2APPENDIX A).

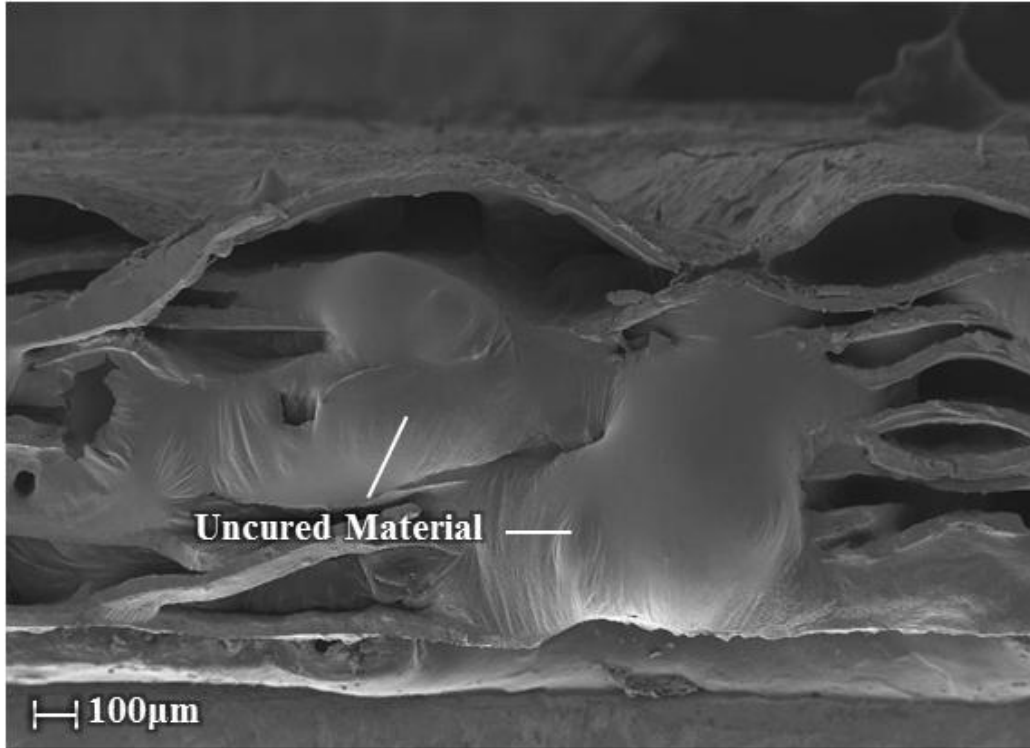


Figure 4-7 Cross sectional view of a Nanocyl 1% (w/v) fractured specimen; at 45X magnification.

Figure 4-8 shows the cross section of a mechanical 2.5% (w/v) Nanocyl specimen. Strings like structures are highlighted in the image. They are appeared to be consolidated strands of material that emerged when the specimen was fractured. Quantitative conclusions as to what these fibers are exactly could not be made. By inspection, the 2.5% (w/v) Nanocyl specimen's layers seem to exhibit much more discrete distortion than that of the 1% (w/v) Nanocyl specimen. The undulated layers of the 1% (w/v) material appear to have larger deflections that may have been caused by the loosening of the polymer matrix as it was heated during processing.

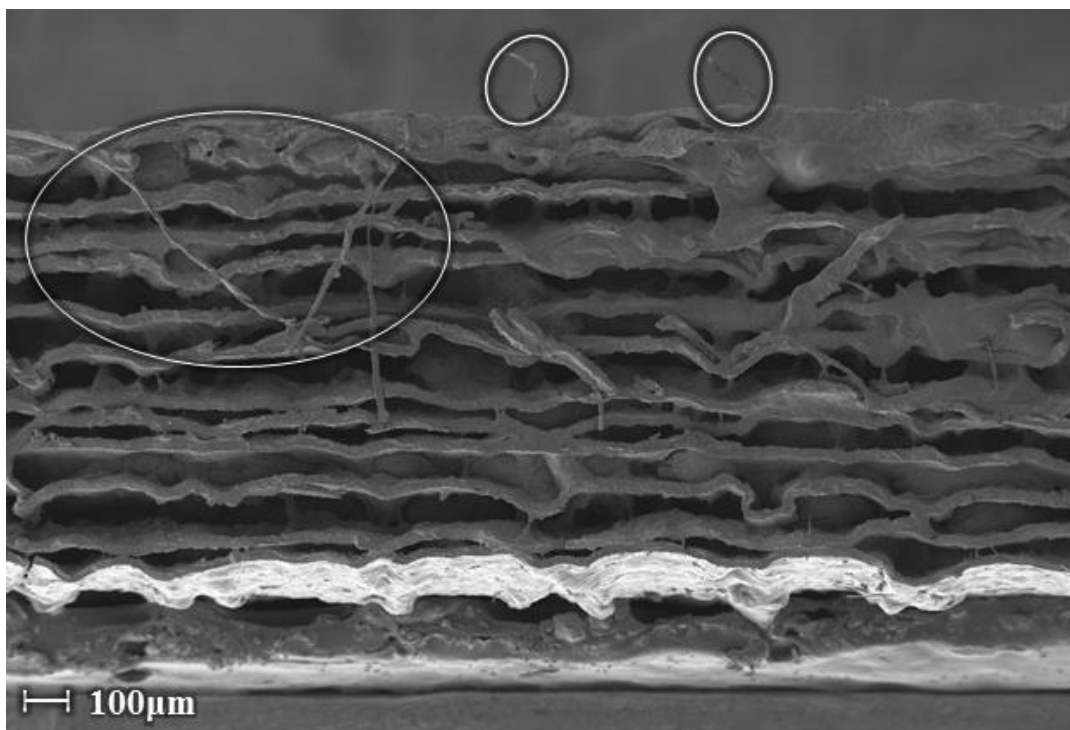


Figure 4-8 Cross sectional view of a Nanocyl 2.5% (w/v) fractured specimen; at 47X magnification.

Further imaging of the 5% (w/v) Nanocyl specimen in Figure 4-9 shows an even larger discrepancy between the uncured and cured material. An analysis of the image shows that the cured layer is $< 20\mu\text{m}$. The negative trend in layer thickness with respect to carbon nanostructure loading continues with the image of a single layer of the PR-24 5% (w/v) specimen shown Figure 4-10. The layer shown in Figure 4-10 appears to be $< 20\mu\text{m}$. At this magnification, similar strand like structures are visible, as in Figure 4-8. This appears to be consolidated bundles of the carbon nanofibers that should be visible at this scale, as they range 50 – 200 μm in length. Also to be noted in Figure 4-10 are the relatively large bubble –like features seen on the top surface of the material. These formations could be a result of the polymer matrix beginning to out gas during heating.

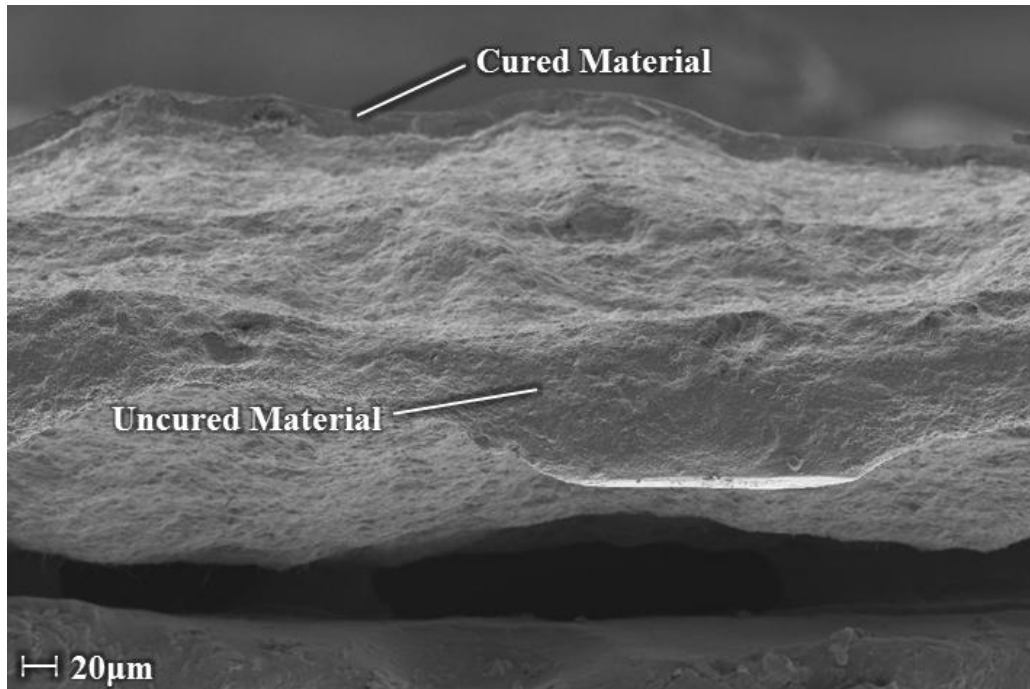


Figure 4-9 Cross sectional view of a Nanocyl 5% (w/v) fractured specimen; at 187X magnification.

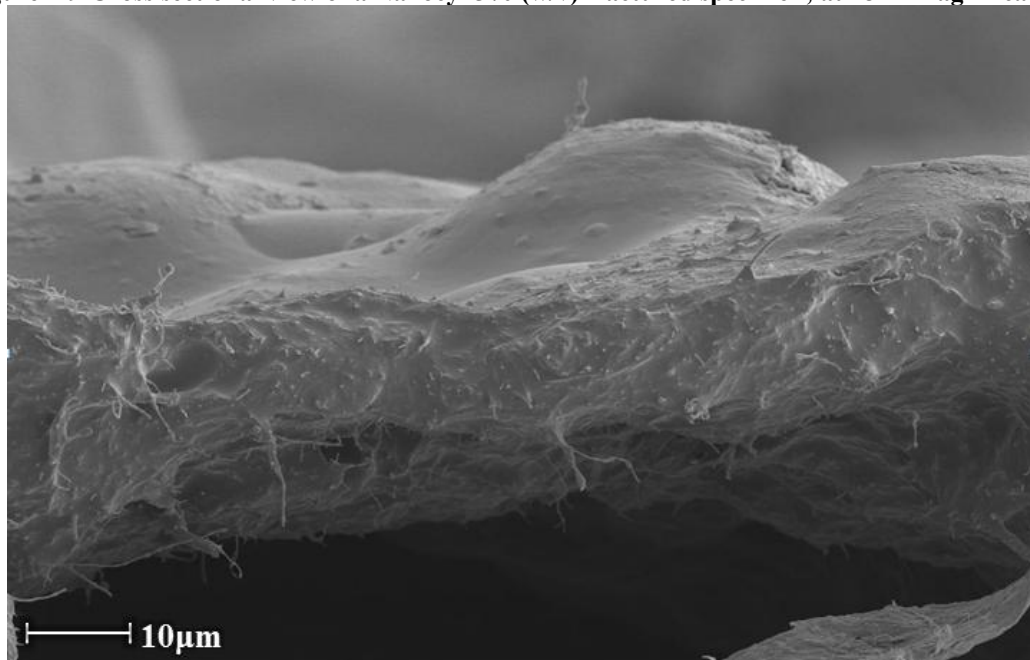


Figure 4-10 Cross sectional view of PR-24 5% (w/v) fractured specimen; at 1,112X magnification.

4.4 THERMAL EVALUATION

A thermal measurement using a photo-differential scanning calorimeter (photo-DSC) was used to track the material's response to phase transitions and chemical reactions as a function of

temperature. The material samples were heated from 0°C to 300°C at a rate of 10°C/min. Four vales were recorded during the process: 1) first endothermic peak 2) second endothermic peak 3) temperature at which material begins to change phase 4) heat capacity (calculated). Figure 4-11 shows the photo-DSC output of the unloaded polymer. Labeled are the recorded points of interest and the data points used to calculate the specific heat. The values are shown in Table 4-3.

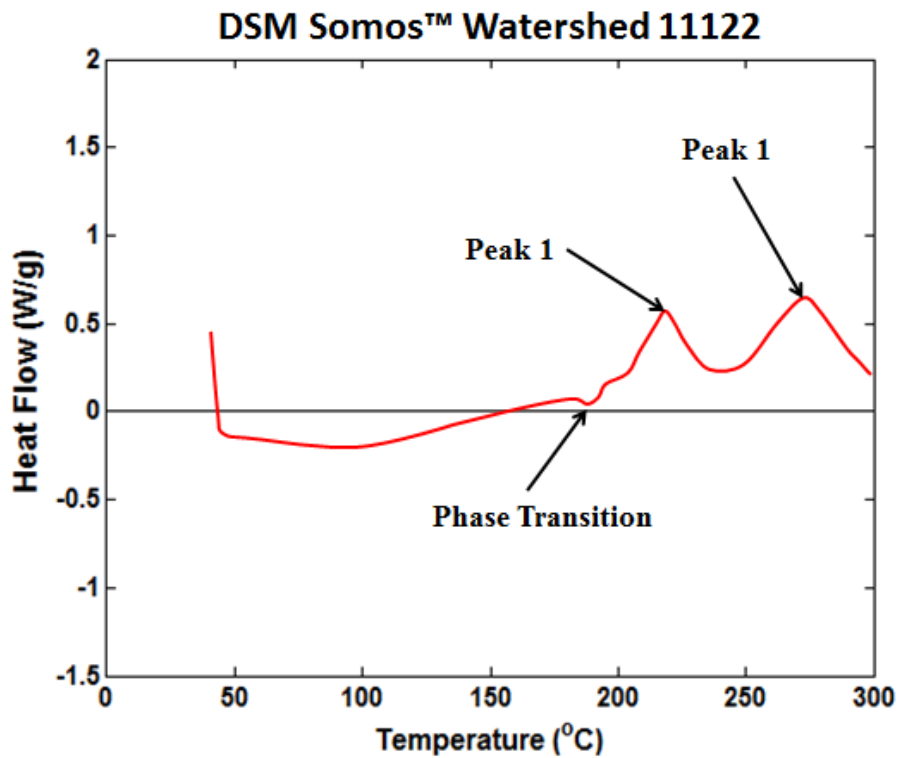


Figure 4-11 Photo-DSC output of DSM Somos™ Watershed 11122

Table 4-3 Measurements of the photo-DSC measurements

	Peak 1	Peak 2	Phase transition	Heat Capacity	Δ Heat Capacity	Δ Phase
Unloaded	216.49 °C	269.89 °C	196.48 °C	162.6 J/g		
1% Nanocyl	230.47 °C	259.66 °C	207.03 °C	335.5 J/g	172.9 J/g	10.55 °C
2.5% Nanocyl	224.81 °C	254.96 °C	201.2 °C	340.3 J/g	177.7 J/g	4.72 °C
5% Nanocyl	236.56 °C	269.29 °C	207.96 °C	254.3 J/g	91.7 J/g	11.48 °C
5% PR-24	234.14 °C	266.56 °C	206.24 °C	338.2 J/g	175.6 J/g	9.76 °C
10% PR-24	220.24 °C	252.89 °C	189.13 °C	370.5 J/g	207.9 J/g	-7.35 °C
				Mean	165.16 J/g	5.83 °C

All the material systems appear to go exhibit an exothermic process during their initial stage of the heating, implying that the material is curing. The insertion of carbon nanostructures produces an average of 165.16 J/g in the change in heat capacity with respect to the unloaded material and a 5.83°C shift in the phase transition. The material with the most carbon nanostructures in it (while not printed), PR-24 10% (w/v) showed the largest change in heat capacity, further reinforcing the witnessed trend. No conclusions could be drawn on the data (i.e. CNT vs CNF) more statistical data is required to the elucidate trends.

As mentioned in section 3.3.2, the operating temperature witnessed on the platform of the UV curing apparatus was around 220°C. At this temperature all the material concentrations were shown to be in an endothermic process. This implies that the elevated temperature the material was introduced to could have begun to rapidly degrade the polymer before it could cross link effectively. This provides insight into the why the material was experiencing delamination as discussed in 3.3.2 and observed in the images provided in 4.3. This observation suggests that the curing process may not be optimal for this polymer system if the temperature cannot be controlled.

CHAPTER 5 CONCLUSIONS

5.1 SUMMARY

This project was an effort to quantify and characterize an approach that would enable the fabrication of parts with an additive manufacturing technique containing high concentrations (<1 % (w/v) of carbon nanostructures. A nanostructure composite was generated out two different carbon structures at different concentrations (1%, 2.5%, 5%, 10% (w/v)) through were successfully mixed into a photo-polymer matrix that would act a carrier and suspension system for the nanostructures. The different mixtures were then shown to be successfully (except for the 10% (w/v)) extruded with a commercial direct printed additive manufacturing system. A UV curing apparatus was set up to act in conjunction with the dispensing system that would polymerize the nanocomposite, solidifying the nanostructures within the matrix. Extruded material was measured through an optical microscope to investigate the repeatable feature size it could produce. This information was then used to fabricated test specimen for mechanical evaluation of the consolidated material.

The mechanical test specimens were put through a fracture evaluation in order to discern their mechanical characteristics. It was observed that the introduction of the carbon nanostructures drastically affected the nanocomposites' ability to efficiently absorb radiated energy and consolidate material. The carbon nanostructures proved to inhibit the polymer's absorptance and minimize its depth penetration, such that uncured material was present between layers of cured material. This was affirmed through imaging of the fractured specimen under a scanning electron microscope.

Furthermore, photo-differential scanning calorimeter measurements of the nanocomposite material revealed that the polymer matrix undergoes an exothermic reaction at $\sim 196^{\circ}\text{C}$. Measurements of the UV curing apparatus platform's temperature fluctuations revealed that it got past the polymer's degradation temperature and was maintained at $\sim 220^{\circ}\text{C}$. It was found that all material concentrations would begin to approach these temperatures if left exposed for more than 15 seconds, upon which it would begin to rapidly distort and delaminate from its substrate. Images generated under SEM showed the material to begin to out gas, forming bubble-like structures on the surface of the material. However, inspection of the of photo-DSC measurements revealed that the introduction of carbon nanostructures to the polymer matrix increased its specific heat by an average of 165.16 J/g across all the concentrations.

5.2 FUTURE WORK

The work performed in this study provides in an insight into some of the challenges involved with attempting to construct three dimensional structures with the carbon nanostructure loaded systems. High loaded ($<1\%$ (w/v)) systems drastically affect the absorptance of the photo-polymer matrix and hinders the system's ability to polymerize effectively. This interaction is primarily a function of two things:

- 1) Energy source's wavelength
- 2) Exposure

A material's response to radiated, electromagnetic energy is predicated on the energy's wavelength. The resin of which this study was focused on is designed for optimal absorbing conditions when exposed to 355nm. In other words, at this wavelength the resin will most effectively begin to polymerize with minimal exposure. The introduction of carbon

nanostructures will alter this because of they are high loss materials (i.e. absorbing), therefore quenching the energy needed for polymerization. These structures also have dimensions that are on the order of the radiation's wavelength. This will introduce geometrical dispersion that is a function of their orientation. An effort to model this interaction may be beneficial in order to better discern the control needed to properly achieve energy penetration or determine if possible.

The energy source used in this project output a full UV spectrum; this is not optimal when trying to design and quantify a repeatable, additive manufacturing process. A quantification of the energy source is also needed to best understand the curing interactions happening during the process. Isolating a wavelength or at least a narrow band of wavelengths allows for measurements of the cured material thickness to be mathematically correlated to the energy and wavelength of the source.

To mechanical effects of the carbon nanostructures within a fully consolidated material were not able to be shown in this study. It has been shown [13, 12, 6] that there are potential benefits for mechanical reinforcement with these structures. A future attempt to consolidate high loadings of carbon nanostructures within a different polymer matrix that requires a different polymerization technique (not necessarily additive) should be attempted. A mechanical evaluation further validating the aforementioned claims will strengthen the need for deeper investigation and development of process methods such as additive manufacturing that have added benefits.

APPENDIX A

This appendix provides the measurement data for the images taken from a SEM. Section A.1 gives the measurements of the line dispense study. Section A.2 shows the measurements done on the fractured specimen.

All the measurements found in this section were done on the original SEM images. Images were input into Solidworks® 2014 as and converted in a drawing file (2D Solidworks® file). The Solidwork® platform is ideal for drawing precise geometrical shapes on the image files. A line was drawn on the scale bar and its dimension was noted (“scale bar length”); this measurement was used as a conversion factor between the geometries drawn on the image and the actual values. The formula in (A.1) shows the conversion between the measured dimensions in Solidworks® and the real units.

$$\text{Actual Dimension} = \frac{\text{CAD Dimension}}{\text{Scale Bar Length}} \times \text{Scale bar value} \quad (\text{A.1})$$

A.1 Line Dispense Study Measurements

Provided list in Table A-1 are the measurements taken during the dispense gap study. The means for each material concentration at the three individual data points is shown, as well as the standard deviations for each that column. An average of the mean was also taken and the standard deviation of the means for each material data set is also shown.

Table A-1 Line measurements and statistical data from dispense gap study

	50	70	100		50	70	100		
Nanocyl 1									
	562.2	579.2	569.5	Mean	562.68	567.78	570.56	Total Mean	567.01
	567.1	552	586.4	Std	25.08	11.42	11.62	Std of Mean	4.00
	576.7	567.2	577.3						
	586.4	578.3	562.2						
	521	562.2	557.4						
Nanocyl 2.5									
	346.5	271.4	237.5	Mean	318.4	283.94	270.775	Total Mean	291.04
	346.5	278.4	247.2	Std	28.18	12.77	43.75	Std of Mean	24.59
	312.6	283.5	264.1						
	305.3	305.3	334.3						
	281.1	281.1	N/A						
Nanocyl 5									
	528.3	540.4	462.8	Mean	527.1	562.68	489.94	Total Mean	526.57
	535.6	588.9	525.8	Std	21.73	27.99	32.97	Std of Mean	36.37
	547.7	584	525.8						
	496.8	574.3	472.5						
	N/A	525.8	462.8						
PR 24 5									
	370.8	346.5	295.6	Mean	363.98	334.4	312.6	Total Mean	336.99
	399.8	339.3	293.2	Std	22.41	11.75	20.07	Std of Mean	25.79
	344.1	315	322.3						
	349	336.8	310.2						
	356.2	334.4	341.7					Mean of Total Means	352.60

**All values shown are in μm*

The profile of the line was estimated by plotting points along the apparent profiles to generate a spline. The cross sectional area was imported into the Solidworks® part modeler and a surface was made from it. A built in area calculator was used to calculate the area. The conversion is similar to (A.1); however, the scale bar length and value were squared to compensate for the area. The values generated through these measurements are shown in Table A-2. Note that the “measured” values are intentionally left without units since they are only representative in the Solidworks® environment.

In Figure A-1 Figure A-4 the dimensional representation of the pen tip used is shown in yellow. The green lines signify the measurement markers; the vertical green line is the midpoint of the measured width. The red line represent the spline profile taken of the line's cross section. In light blue is the CAD dimension of the scale bar.

Table A-2 Line cross-section measurements

	Nanocyl 1%	Nanocyl 2.5%	Nanocyl 5%	PR - 24 5%
Scale Bar Length	57.70	73.72	57.85	59.16
Scale Bar Value	100 μm	100 μm	100 μm	100 μm
Measured Width	300.63	262.15	279.37	233.71
Measured Thickness	84.352	34.954	57.694	30.880
Actual Width	521.01 μm	355.59 μm	482.93 μm	395.07 μm
Actual Thickness	146.19 μm	47.41 μm	99.73 μm	52.20 μm
Measured X - Area	19,363.85	10,285.24	12,181.32	6,503.58
Actual X - Area	58,160.34 μm^2	18,924.06 μm^2	36,398.89 μm^2	18,584.32 μm^2

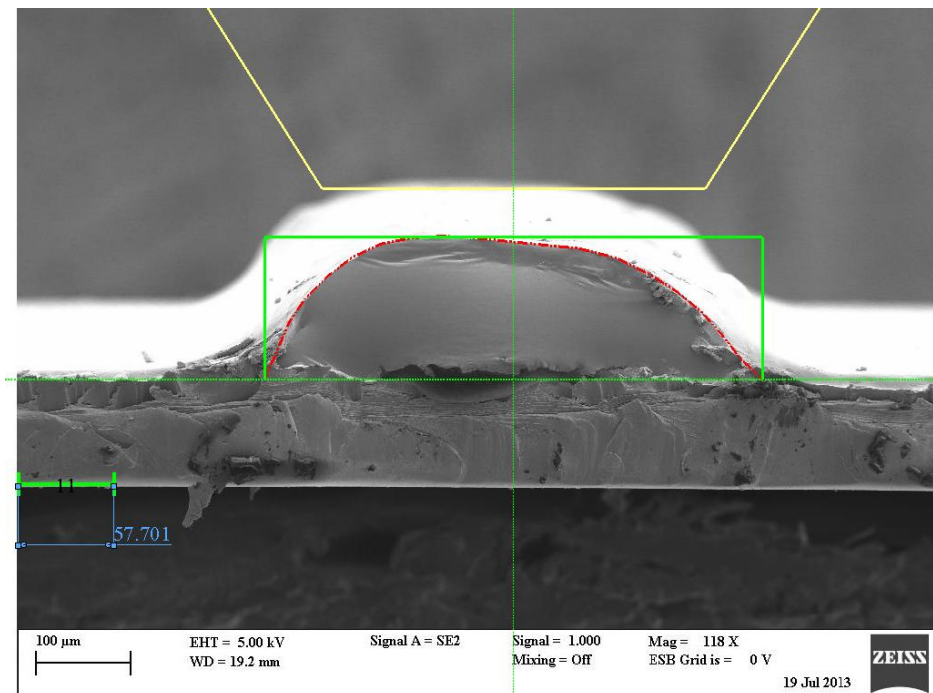


Figure A-1 Cross section of Nanocyl 1% (w/v)

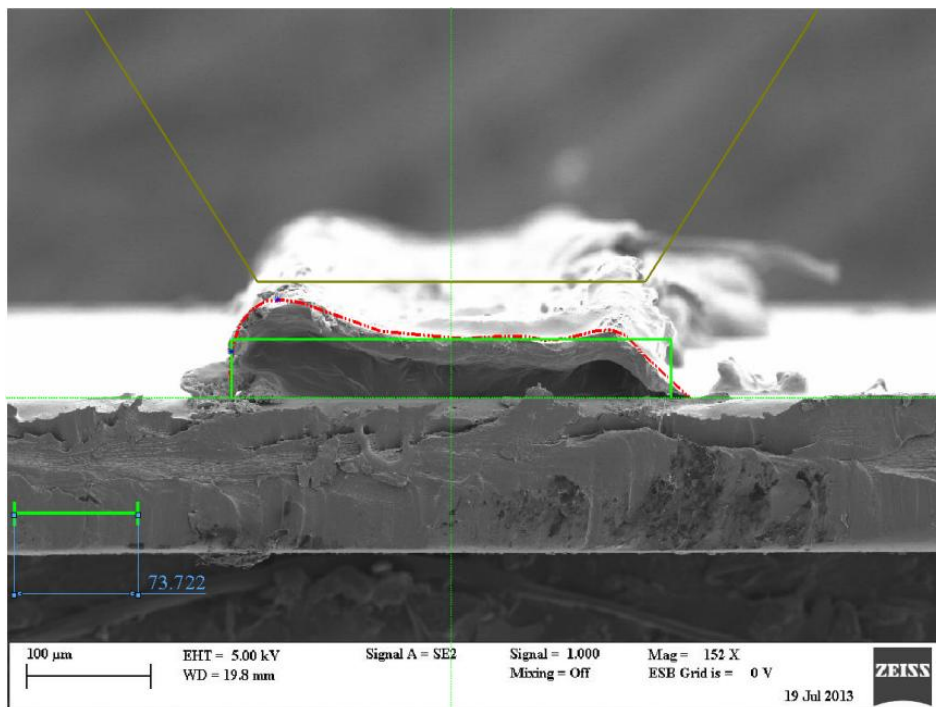


Figure A-2 Cross section of Nanocyl 2.5% (w/v)

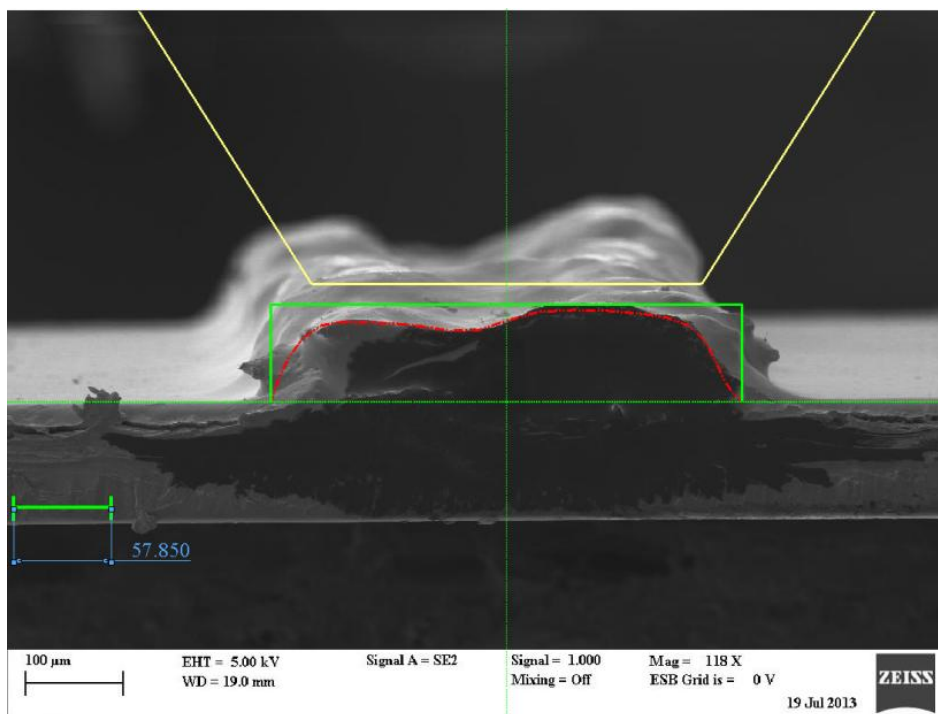


Figure A-3 Cross section of Nanocyl 5% (w/v)

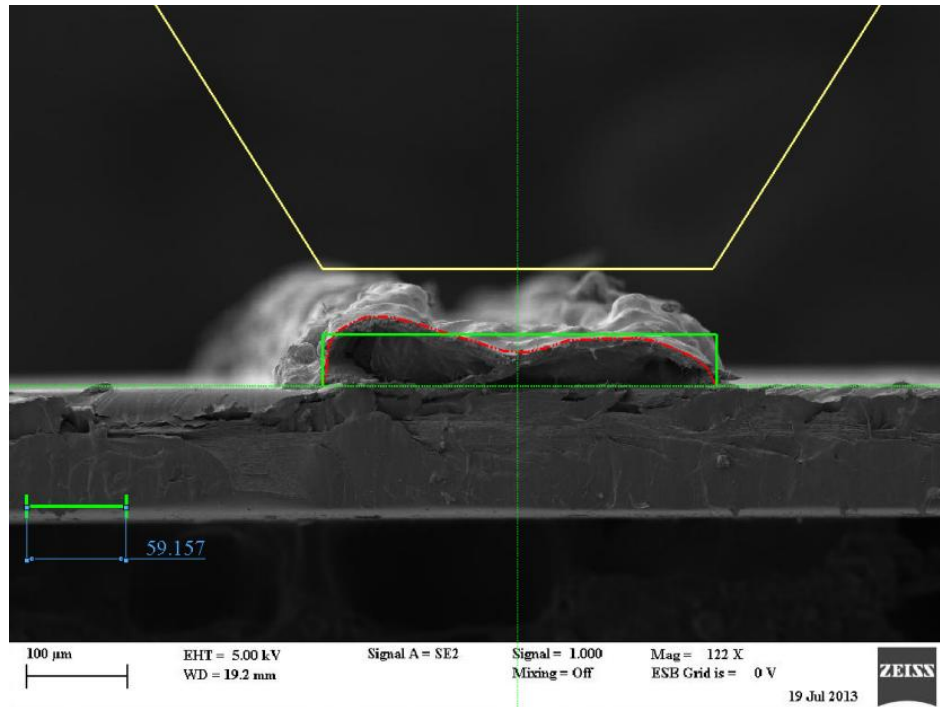


Figure A-4 Cross section of PR – 24 5% (w/v)

A.2 Fracture Specimen Measurements

Table A-3 Measurements of the layers of the fractured specimen
1 % Nanocyl

Layer	Scale Bar Length	Scale Bar Value	Measured	Real Thickness
1	0.37	100	0.24	64.86 μm
2	0.37	100	0.23	62.16 μm
3	0.37	100	0.17	45.95 μm
4	0.37	100	0.21	56.76 μm
5	0.37	100	0.19	51.35 μm
6	0.37	100	0.15	40.54 μm
7	0.37	100	0.15	40.54 μm
8	0.37	100	0.17	45.95 μm
Mean				51.01 μm
Std. Dev.				8.80 μm

2.5 % Nanocyl

Layer	Scale Bar Length	Scale Bar Value	Measured	Real Thickness
1	0.39	100	0.16	41.03 μm
2	0.39	100	0.14	35.90 μm

3	0.39	100	0.09	23.08	μm
4	0.39	100	0.1	25.64	μm
5	0.39	100	0.16	41.03	μm
6	0.39	100	0.12	30.77	μm
7	0.39	100	0.12	30.77	μm
8	0.39	100	0.17	43.59	μm
9	0.39	100	0.14	35.90	μm
10	0.39	100	0.19	48.72	μm
11	0.39	100	0.12	30.77	μm
12	0.39	100	0.32	82.05	μm
Mean				39.10	μm
Std. Dev.				14.81	μm

APPENDIX B

Table B-1 Test specimen build parameters

	Nanocyl 1%	Nanocyl 2.5%	Nanocyl 5%	PR – 24 5%
Print Speed 0°	70 mm/s	70 mm/s	70 mm/s	70 mm/s
Print Speed 90°	50 mm/s	50 mm/s	50 mm/s	50 mm/s
Valve Speed	8 mm/s	8 mm/s	8 mm/s	8 mm/s
Valve Opening	0.3 mm	0.3 mm	0.3 mm	0.3 mm
Valve Wait	0.01 seconds	0.01 seconds	0.01 seconds	0.01 seconds
Pressure	12 psi	50 psi	20 psi	50 psi
Cure Time	~15 seconds	~10 seconds	~5 seconds	~10 seconds

Table B-2 Raw data and measurements of layers during mechanical specimen build

Nanocyl 1% (w/v)			Nanocyl 2.5% (w/v)						Nanocyl 5% (w/v)			PR – 24 5% (w/v)		
Specimen 1			Specimen 1		Specimen 2		Average		Specimen 1			Specimen 1		
(mm)	(µm)	(µm)	(mm)	(µm)	(mm)	(µm)	(µm)	(µm)	(mm)	(µm)	(µm)	(mm)	(µm)	(µm)
-78.871	0	167	-78.846	0	-78.895	0	0	108	-78.888	0	253	-78.904	0	68
-78.704	167	177	-78.774	72	-78.751	144	108	64.5	-78.635	253	117	-78.836	68	102
-78.527	344	64	-78.719	127	-78.677	218	172.5	80	-78.518	370	135	-78.734	170	83
-78.463	408	172	-78.627	219	-78.609	286	252.5	67.5	-78.383	505	189	-78.651	253	80
-78.291	580	64	-78.558	288	-78.543	352	320	84	-78.194	694	64	-78.571	333	81
-78.227	644	98	-78.446	400	-78.487	408	404	88.5	-78.13	758	133	-78.49	414	77
-78.129	742	153	-78.341	505	-78.415	480	492.5	68.5	-77.997	891	122	-78.413	491	69
-77.976	895	45	-78.269	577	-78.35	545	561	79.5	-77.875	1013		-78.344	560	93
-77.931	940	148	-78.193	653	-78.267	628	640.5	56.5				-78.251	653	80
-77.783	1088		-78.134	712	-78.213	682	697	85				-78.171	733	77
			-78.034	812	-78.143	752	782	83				-78.094	810	97
			-77.971	875	-78.04	855	865	97.5				-77.997	907	103
			-77.883	963	-77.933	962	962.5	113.5				-77.894	1010	
			-77.748	1098	-77.841	1054	1076							
	Mean	120.89					Mean	82.77		Mean	144.71		Mean	84.17
	Std	52.93					Std	16.62		Std	60.16		Std	11.89
Raw Data			Aggregated Thicknesses		Layer Differences		Final Thickness							

APPENDIX C

All values shown in the ensuing tables were taken in the tensile direction. The strain and stress values were calculated to be tensile values, not true values. The acronym T.S. stands for Tensile Strength.

Table C-1 Results of mechanical experiments for the unloaded DSM Somos™ Watershed 11122.

Unloaded Polymer

	Young's Modulus	Load at T.S.	Extension at T.S.	Strain at T.S.	Stress at T.S.	Time at T.S.
	(TPa)	(N)	(mm)	(mm/mm)	(MPa)	(seconds)
	2.8251	237.7275	1.0768	0.0180	39.6213	0.2388
	2.7453	276.7269	1.1824	0.0197	46.1212	0.2598
	3.1787	362.7221	1.5081	0.0251	60.4537	0.3248
	3.4536	367.8140	1.6283	0.0271	61.3023	0.3488
	3.1395	327.2562	1.7034	0.0284	54.5427	0.3638
Mean	3.0684	314.4493	1.4198	0.0237	52.4082	0.3072
Std. Dev.	0.2869	56.2390	0.2765	0.0046	9.3732	0.0552

Table C-2 Results of mechanical experiments for 1% (w/v) Nanocyl nanocomposite

1% Nanocyl

Load at T.S.	Extension at T.S.	Strain at T.S.	Stress at T.S.	Time at T.S.
(N)	(mm)	(mm/mm)	(MPa)	(sec)
1.82772	9.88339	0.16472	0.21759	2

**Only one value of this loading was suitable for testing.*

Table C-3 Results of mechanical experiments for 2.5% (w/v) Nanocyl nanocomposite

2.5% Nanocyl

Young's Modulus	Load at T.S.	Extension at T.S.	Strain at T.S.	Stress at T.S.	Time at T.S.
(MPa)	(N)	(mm)	(mm/mm)	(MPa)	(sec)

	80.76	15.64	1.38	0.02	1.86	0.30
	96.96	24.69	1.82	0.03	2.94	0.39
	86.40	13.70	1.38	0.02	1.63	0.30
Mean	88.04	18.01	1.53	0.03	2.14	0.33
Std. Dev.	6.72	5.86	0.25	0.00	0.70	0.05

**Table C-4 Results of mechanical experiments for 5% (w/v) Nanocyl nanocomposite
5% Nanocyl**

	Young's Modulus	Load at T.S.	Extension at T.S.	Strain at T.S.	Stress at T.S.	Time at T.S.
	(MPa)	(N)	(mm)	(mm/mm)	(MPa)	(sec)
	35.098	3.641	0.880	0.015	0.434	0.200
	45.882	8.036	1.383	0.023	0.957	0.300
Mean	40.490	5.839	1.132	0.019	0.695	0.250
Std. Dev.	5.392	3.107	0.356	0.006	0.370	0.071

**Table C-5 Results of mechanical experiments for 5% (w/v) PR-24 nanocomposite
5% PR - 24**

	Young's Modulus	Load at T.S.	Extension at T.S.	Strain at T.S.	Stress at T.S.	Time at T.S.
	(MPa)	(N)	(mm)	(mm/mm)	(MPa)	(sec)
	68.06	3.38	0.36	0.01	0.40	0.10
	47.22	5.82	0.88	0.01	0.69	0.20
Mean	57.64	4.60	0.62	0.01	0.55	0.15
Std. Dev.	10.42	1.72	0.37	0.01	0.20	0.07

REFERENCES

- [1] E. Hosbawm, *Industry and Empire: The Birth of the Industrial Revolution*, The New Press, 1999.
- [2] R. Lucas, "The Industrial Revolution: Past and Future," The Federal Reserve Bank of Minneapolis, Minneapolis., 2003.
- [3] B. Ryder, "The Third Industrial Revolution," *The Economist*, 21 April 2012.
- [4] D. L. Bourell, J. J. Beaman, M. C. Leu and D. W. Rosen, "A Brief History of Additive Manufacturing and the 2009 Roadmap for Additive Manufacturing: Looking Back and Looking Ahead," in *RapidTeach 2009*, Istanbul, 2009.
- [5] J. N. Coleman, U. Khan and Y. K. Gun'ko, "Mechanical Reinforcement of Polymers Using Carbon Nanotubes," *Advanced Materials*, vol. 18, no. 6, pp. 689-706, 2006.
- [6] J. N. Coleman, U. Khan, W. J. Blau and Y. K. Gun'ko, "Small but strong: A review of the mechanical properties of carbon nanotube-polymer composites," *Carbon*, vol. 44, no. 9, pp. 1624-1652, 2006.
- [7] Y. Geng, M. Liu, J. Li, X. Shi and J. Kim, "Effects of surfactant treatment on mechanical and electrical properties of CNT/epoxy nanocomposites," *Composites A*, vol. 39, no. 12, pp. 1876-1883, 2008.
- [8] J. Kim and P.-C. Ma, *Carbon Nanotubes for Polymer Reinforcement*, Boca Raton: Taylor & Francis, 2011.
- [9] P.-C. Ma, N. A. Siddiqui, G. Marom and J.-K. Kim, "Dispersion and functionalization of carbon nanotubes for polymer-based nanocomposites: A review," *Composites Part A: Applied Science and Manufacturing*, vol. 41, no. 10, pp. 1345-1367, 2010.
- [10] W. Callister, *Materials Science and Engineering*, Wiley, 2007.
- [11] I. Gibson, B. Stucker and W. D. Rosen, *Additive Manufacturing Technologies: Rapid Prototyping to Direct Digital Manufacturing*, Springer, 2010.
- [12] H. Sandoval, *Functionalizing Epoxy-Based Stereolithography Resins Using Multi-Walled Carbon Nanotubes*, Master's Thesis, University of Texas at El Paso, 2006.
- [13] J. Sandoval and R. Wicker, "Funtinoalizing stereolithography resins: effects of dispersed multi-walled carbon nanotubes on physical properties," *Rapid Prototyping Journal*, vol. 12, no. 5, pp. 292-303, 2006.
- [14] ASTM F42.91 Subcommittee, "Standard Terminology for Additive Manufacturing Technologies," 2011.
- [15] J. P. Wachsmuth, *Multiple Independent Extrusion Heads for Fused Deposition Modeling*, Blacksburg: Virginia Polytechnic Institute and State University, 2008.
- [16] P. J. Bàrtolo, *Stereolithography*, New York: Springer, 2011.
- [17] J. P. Kruth, G. Levy and T. Childs, "Consolidation phenomena in laser and powder-bed based layered manufacturing," *CIRP Annals - Manufacturing Technology*, vol. 56, no. 2, pp. 730-759, 2007.
- [18] Z. H. Liu, J. J. Nolte, J. Packard, G. Hilmas, F. Dogan and M. C. Leu, "Selective Laser

- Sintering of High Density Alumina Ceramic Parts," in *Proceedings of the 35th International MATADOR Conference*, 2007.
- [19] S. Kenzari, D. Bonina, J. M. Dubois and V. Fomèe, "Complex Metallic Alloy as New Materials for Additive Manufacturing," *Science and Technology of Advanced Materials*, vol. 15, no. 2, 2014.
- [20] M. J. Mireles, D. Espalin, D. Roberson, B. Zinniel, F. Medina and R. B. Wicker, "Fused Deposition Modeling of Metals," in *Solid Freeform Symposium*, Austin, 2012.
- [21] K. Buyukhatipoglu, "Bioprinted Superparamagnetic Nanoparticles for Tissue Engineering Applications: Synthesis, Cytotoxicity Assessment, Novel Hybrid Printing System," Drexel University, Philadelphia, 2009.
- [22] C. Norotte, F. Marga, L. Niklason and G. Forgacs, "Scaffold-Free Vascular Tissue Engineering Using Bioprinting," *Biomaterials*, vol. 30, no. 30, pp. 5910-5917, 2009.
- [23] J. E. Blather, "Manufacture of Contour Relief Maps". US Patent 473,901, 1892.
- [24] B. Perera, "Process of Making Relief Maps". US Patent 2,189,592, 1940.
- [25] C. Baese, "Photographic Process for the Reproduction of Plastic Objects". US Patent 774,549, 1904.
- [26] K. Matsubara, "Molding Method of Casting Using Photocurable Substance". Japan Patent Sho 51[1976]-10813, 1974.
- [27] I. Morioka, "Process for Manufacturing a Relief by the Aid of Photography". US Patent 2,015,457, 1935.
- [28] I. Morioka, "Process for Plastically Reproducing Objects". US Patent 2,250,796, 1944.
- [29] W. Swainson, "Method, Medium and Apparatus for Producing Three-Dimensional Figure Product". US Patent 4,041,476.
- [30] A. Herbert, "Solid Object Generation," *Journal of Applied Photographic Engineering*, vol. 8, no. 4, pp. 185-188, 1982.
- [31] H. Kodama, "Automatic Method for Fabricating a Three-Dimensional Plastic Model with Photo Hardening Polymer," *Review of Scientific Instruments*, vol. 52, pp. 1770-1773, 1981.
- [32] Y.-L. Zhang, Q.-D. Chen, H. Xia and H.-B. Sun, "Designable 3D nanofabrication by femtosecond laser direct writing," *nanotoday*, vol. 5, no. 5, pp. 435-448, 2010.
- [33] L. Li and J. T. Fourkas, "Multiphoton Polymerization," *Materials Today*, vol. 10, no. 6, pp. 30-37, 2007.
- [34] J. W. Judy, "Microelectromechanical systems (MEMS): fabrication, design and applications," *Smart Materials and Structures*, vol. 10, no. 6, pp. 1115-1134, 2001.
- [35] M. Vaezi, S. Chianrabutra, B. Mellor and S. Yang, "Multiple material additive manufacturing – Part 1: a review," *Virtual and Physical Prototyping*, vol. 8, no. 1, pp. 19-50, 2013.
- [36] K. V. Wong and A. Hernandez, "A Review of Additive Manufacturing," *ISRN Mechanical Engineering*, vol. 208760, p. 10, 2012.
- [37] Materialise, [Online]. Available: <http://software.materialise.com/magics>. [Accessed July 2014].
- [38] Stratasys, [Online]. Available: www.stratasys.com. [Accessed July 2014].
- [39] C.-J. Bae and H. J. W., "Integrally Cored Ceramic Mold Fabricated by Ceramic

- Stereolithography," *Applied Ceramic Technology*, vol. 8, no. 6, pp. 1255-1262, 2011.
- [40] P. F. Jacobs, "Rapid Prototyping & Manufacturing: Fundamentals of Stereolithography," in *Basic Polymer Chemistry*, Dearborn, Society of Manufacturing Engineers, 1992, pp. 25-58.
- [41] A. Reiser, *Photosensitive Polymers*, New York: Wiley, 1989.
- [42] J. Crivello and J. Lee, "Synthesis, characterization, and photoinitiated cationic polymerization of silicon-containing epoxy resins," *J. Polym. Sci. Part A: Polymer Chemistry*, vol. 28, pp. 479-503, 1990.
- [43] K. H. Church, C. Fore and T. Feeley, "Commercial applications and review for direct write technologies," in *MRS Proceedings on Materials Development for Direct Write Technologies*, San Francisco, 2000.
- [44] A. Piquè and D. Chrissey, *Direct- Write Technologies for Rapid Prototyping Applications*, San Diego: Academic Press, 2002.
- [45] D. B. Chrissey, "The Power of Direct Writing," *Science*, vol. 289, no. 5481, pp. 879-881, 2000.
- [46] R. Terrill, "Laser ablation patterning for low cost 3D die packaging," *IEEE Aerospace Conference Proceedings*, pp. 481-488, 1997.
- [47] L. Mortara, J. Hughes, P. Ramsundar, F. Livesey and D. Probert, "Proposed classification scheme for direct writing technologies," *Rapid Prototyping Journal*, vol. 15, no. 4, 2009.
- [48] M. Heule, S. Vuillemin and L. Gauckler, "Powder Based Ceramic Meso- and Microscale Fabrication Process," *Advanced Materials*, vol. 15, no. 15, pp. 1237-1245, 2003.
- [49] H. Herman, "Plasma Sprayed Coatings," *Scientific American*, vol. 259, no. 3, pp. 112-117, 1988.
- [50] nScrypt, [Online]. Available: www.nscrypt.com. [Accessed July 2014].
- [51] R. Taylor, K. Church, J. Culver and S. Eason, "Direct-write techniques for fabricating unique antennas," in *MRS Proceeding on Materials Development for Direct Write Technologies*, San Francisco, 2000.
- [52] P. I. Deffenbaugh, R. C. Rumpf and K. H. Church, "Broadband Microwave Frequency Characterization of 3-D Printed Materials," *IEEE Transactions on Components, Packaging and Manufacturing Technology*, vol. 3, no. 12, pp. 2147-2155, 2013.
- [53] J. A. Lewis and G. M. Gratson, "Direct writing in three dimensions," *Materials Today*, vol. 7, no. 7-8, pp. 32-39, 2004.
- [54] J. Lewis, "Direct-write assembly of ceramics from colloidal inks," *Current Opinion in Solid State and Material Science*, vol. 6, no. 3, pp. 245-250, 2002.
- [55] G. Gratson, J. Lewis and M. Xu, "Microperiodic structures: Direct writing of three-dimensional webs," *Nature*, vol. 428, no. 386, 2004.
- [56] B. Li, P. Clark and K. Church, "Robust Direct-Write dispensing tool and solutions for micro/meso-scale manufacturing and packaging," in *International Manufacturing Science and Engineering Conference*, Atlanta, 2007.
- [57] A. Ehsani and M. Kesler, "Laser speed up board production," *IEEE Spectrum*, vol. 37, no. 5, 2000.
- [58] X. Chen, K. Church and Y. H., "High speed non-contact printing for solar cell front side metallization," in *IEEE Photovoltaic Specialist Conference*, Honolulu, 2010.

- [59] K. Church, E. MacDonald, P. Clark, R. Taylor, K. Stone, M. Wilhelm, F. Medina, J. Lyke and R. Wicker, "Printed electronic processes for flexible hybrid circuits and antennas," in *Flexible Electronics & Displays Conference and Exhibition*, Phoenix, 2009.
- [60] L. Griffith and G. Naughton, "Tissue Engineering - Current Challenges and Expanding Opportunities," *Science*, vol. 295, no. 5557, pp. 1009-1014, 2002.
- [61] Y. e. a. Li, "KCNQ1 Gain-of-function mutation in familial atrial fibrillation," *Science*, vol. 299, no. 5604, p. 251-254, 2003.
- [62] D. Therriault, S. White and J. Lewis, "Chaotic mixing in three-dimensional microvascular networks fabricated by direct-write assembly," *Nature Materials*, vol. 2, pp. 265-271, 2003.
- [63] Y. Lee and B. P., "Tunable Inverse Opal Hydrogel pH Sensors," *Advanced Materials*, vol. 15, no. 7-8, pp. 563-566, 2003.
- [64] J. Joannopoulos, P. Villeneuve and S. Fan, "Photonic crystals: putting a new twist on light," *Nature*, vol. 386, pp. 143-149, 1997.
- [65] M. Meyyapan, *Carbon Nanotubes: Science and Application*, Boca Raton: CRC Press, 2005.
- [66] M. Monthieux, "Who should be given the credit for the discovery of carbon nanotubes," *Carbon*, vol. 44.9, pp. 1621-1623, 2006.
- [67] M. Endo, K. Takeuchi, K. Kobori, K. Takahasi, H. Kroto and A. Sarkar, "Pyrolytic carbon nanotubes from vapor grown carbon fibers," *Carbon*, vol. 33, pp. 873-881, 1995.
- [68] P. J. F. Harris, *Carbon Nanotubes and Related Structures - New Materials for the Twenty-first Century*, Cambridge: Cambridge University Press, 1999.
- [69] S. Iijima, "Helical microtubules of graphite carbon," *Nature*, vol. 354, pp. 56-58, 1991.
- [70] S. Reich, C. Thomsen and J. Maultzsch, *Carbon Nanotubes - Basic Concepts and Physical Properties*, Weinheim: Wiley-VCH, 2004.
- [71] M. O'Connell, *Carbon Nanotubes: Properties and Applications*, Boca Raton: Taylor and Francis, 2006.
- [72] K. Teo, C. Singh, M. Chhowalla and W. Milne, "Catalytic Synthesis of Carbon Nanotubes and Nanofibers," *Encyclopedia of Nanoscience and Nanotechnology*, vol. X, pp. 1-22, 2003.
- [73] K. Nordheim, "Growth and Properties of Carbon Nanotubes," Norwegian University of Science and Technology, Trondheim, Norway, 2012.
- [74] Y. Kin, T. Hayashi, M. Enod and M. Dresselhaus, "Carbon Nanofibers," in *Springer Handbook of Nanomaterials*, Springer, 2011, pp. 233-258.
- [75] W. Zhong, F. Li, Z. Zhang, L. Song and Z. Li, "Short fiber reinforced composites for fused deposition modeling," *Materials Science and Engineering A*, vol. 301, no. 2, pp. 125-130, 2001.
- [76] M. Shofner, K. Lozan, F. Rodriguez-Macias and E. Barrera, "Nanofiber-Reinforced Polymers Prepared by Fused Deposition Modeling," *Journal of Applied Polymer Science*, vol. 89, no. 11, pp. 3081-3090, 2002.
- [77] D. Karalekas and K. Antoniou, "Composite rapid prototyping: overcoming the drawback of poor mechanical properties," *Journal of Material Processing Technology*, Vols. 153-154, pp. 526-530, 2004.
- [78] M. Griffith and J. Halloran, "Freeform fabrication of ceramics via Stereolithography," *Journal of American Ceramics Society*, vol. 79, no. 10, pp. 2601-2608, 1996.

- [79] C. Corcione, A. Greco, F. Montagna, A. Licciulli and A. Maffezzoli, "Silica moulds built by stereolithography," *Journal of Materials Science*, vol. 40, no. 18, pp. 4899-4904, 2005.
- [80] DSM, [Online]. Available: http://www.dsm.com/products/somos/en_US/offerings/Somos-NanoTool.html?download-file-url=http%3A%2F%2Fwww.dsm.com%2Fcontent%2Fdam%2Fdsm%2Fsomos%2Fen_US%2Fdocuments%2FBrand-Status-Product-Datasheets%2FUS%2520English%2520-%2520A4%2FSomos%2520NanoTool%2520Dat. [Accessed July 2014].
- [81] DSM Corporation, "Somos® Watershed™ 11122 datasheet," 2014.
- [82] Nanocyl™, [Online]. Available: www.nanocyl.com. [Accessed July 2014].
- [83] Nanocyl™, "Nanocyl™ NC 7000 Datasheet," 2009-V05.
- [84] Pyrograf Products Inc., "Pyrograf®-III Datasheet," [Online]. Available: http://pyrografproducts.com/nanofiber.html#_PR-24-XT-HHT_Data_Sheet. [Accessed July 2014].
- [85] A. Datar, "Micro-extrusion process parameter modeling," *Thesis. Rochester Institute of Technology*, 2012.
- [86] American Ultraviolet, [Online]. Available: <http://www.americanultraviolet.com/uv-curing-solutions/>. [Accessed July 2014].
- [87] P. Mills and J. Raymont, "Ultraviolet Measurement for Formulators: Part I," *Paint and Coatings Industry Magazine*, 2009.
- [88] Micro-Epsilon America, [Online]. Available: www.micro-epsilon.com. [Accessed July 2014].
- [89] Micro-Epsilon, "thermoMeter CTM-3 Datasheet," 2008.
- [90] U. Lakshminarayan, S. Ogrydziak and H. L. Marcus, "Selective Sintering of Ceramic Materials," *Dissertation Abstracts International (USA)*, vol. 53, no. 4, p. 215, 1992.
- [91] S. Kalenik and B. Anderson, "Design Economics of Surface Mount PCBs," *Circuit World*, vol. 12, no. 1, pp. 26-28, 1985.
- [92] A. J. Lopes, E. MacDonald and R. B. Wicker, "Integrating stereolithography and direct print technologies for 3D structural electronics fabrication," *Rapid Prototyping Journal*, vol. 18, no. 2, pp. 129-143, 2012.
- [93] A. E. Ruehli, G. Antonini, J. Esch, J. Ekman, A. Mayo and A. Orlandi, "Nonorthogonal PEEC Formulation for Time and Frequency Domain EM and Circuit Modeling," *IEEE Transactions on Electromagnetic Compatibility*, vol. 45, no. 2, pp. 167-176, 2003.
- [94] M. del Mar Hershenson, S. S. Mohan, S. P. Boyd and T. H. Lee, "Optimization of inductor circuits via geometric programming," in *IEEE on Design Automation Conference Proceeding 36th*, New Orleans, 1999.
- [95] W. Smith, "High Frequency 3D Simulations for High Frequency 3D Printed Electronics," in *IMAPS Advanced Technology Workshop on 3D and Conformable Printed Electronic Packaging*, El Paso, 2012.
- [96] Y. Ling, H. Zhang, G. Gu, X. Lu, V. Kayastha, C. S. Jones, W.-S. Shih and D. C. Janzen, "A Printable CNT Based FM Passive Wireless Sensor Tag on a Flexible Substrate With Enhanced Sensitivity," *IEEE Sensor Journal*, vol. 14, no. 4, pp. 1193-1197, 2014.
- [97] N. G. Sahoo, S. Rana, J. W. Cho, L. Li and S. H. Chan, "Polymer nanocomposites based on

- functionalized carbon nanotubes," *Progress in Polymer Science*, vol. 35, no. 7, pp. 837-867, 2010.
- [98] C. Buzea, I. I. Pacheco and K. Robbie, "Nanomaterials and nanoparticles: Sources and Toxicity," *Biointerphases*, vol. 2, no. 4, pp. MR17-MR-71, 2007.
- [99] "Proceedings of the Solid Freeform Fabrication Symposium," in *Mechanical Engineering Department; University of Texas*, Austin, 1990-2013.
- [10] T. Gaskin, "Earth Science Teaching Device". Patent 3,751,827, 1973.
0]
- [10] E. Zang, "Vitavue Relief Model Technique". US Patent 3,137,080, 1964.
1]
- [10] 3D Systems, [Online]. Available: <http://www.3dsystems.com/>. [Accessed July 2014].
2]
- [10] Optomec, [Online]. Available: www.optomec.com. [Accessed July 2014].
3]
- [10] Sciaky, [Online]. Available: www.sciaky.com. [Accessed July 2014].
4]
- [10] ExOne, [Online]. Available: www.exone.com. [Accessed July 2014].
5]
- [10] Solido, [Online]. Available: www.solido3d.com. [Accessed July 2014].
6]
- [10] EnvisionTEC, [Online]. Available: www.envisiontec.com. [Accessed July 2014].
7]
- [10] EOS, [Online]. Available: www.eos.info/en. [Accessed July 2014].
8]
- [10] Fabrisonic, [Online]. Available: <http://www.fabrisonic.com>. [Accessed July 2014].
9]
- [11] S. Kannan and S. D., "Assessment of Mechanical Properties of Ni-coated ABS Plastics using FDM Process," *International Journal of Mechanical & Mechatronics Engineerings*, vol. 14, no. 03, pp. 30-35, 2014.
- [11] W. Schnabel, *Polymers and Light: Fundamentals and Technical Applications*, Königswinter 1] : Wiley-VCH, 2007.
- [11] Y. Tang, *Stereolithography Cure Process Modeling*, Dissertation, Georgia Institute of 2] Technology, 2005.
- [11] S. Kuebler, M. Rumi, T. Watanbe, K. Braun, B. H. A. Crumpston, L. Erksine, S. 3] Thayumanavan, S. Barlow, S. Marder and J. Perry, "Optimizing two photon initiators and exposure conditions for three dimensional lithographic microfabrication," *Journal of Photopolymer Science Technology*, vol. 14, no. 657, pp. 1-5, 2001.
- [11] V. Popov, "Carbon Nanotubes: properties and application," *Materials Science and 4] Engineering*, vol. 43, pp. 61-102, 2004.
- [11] O. Ivanova, C. Williams and T. Campbell, "Additive manufacturing and nanotechnology: 5] promises and challenges," *Rapid Prototyping Journal*, vol. 19, no. 5, pp. 353-364, 2013.
- [11] B. Li, W. Wood, L. Barker, G. Sui, C. Leer and W. Zhong, "Highly improved mechanical

- 6] and tribological properties in nanofiber composites," Society of Plastics Engineers, 2012.
- [11 Pyrograf Products Inc., [Online]. Available: www.pyrografproducts.com. [Accessed July 7] 2014].
- [11 B. Blackburn, M. Camratta and E. Wachsman, "Advances in Rapid Prototyping for Solid State Ionics," *ECS Transactions*, vol. 16, no. 51, pp. 367-379, 2009.
- [11 D. Liu, S. Matthews, C. Zhang and M. Duignan, "Laser Direct-Write Technology and Its Low Processing Temperature Low Cost Applications," *IMAPS Advancing Microelectronics*, vol. 29, no. 2, 2002.

CURRICULUM VITAE

Ricardo X. Rodriguez was born in Caracas, VZ in 1989. After spending the majority of his life in Pembroke Pines, FL, he moved to Orlando, FL to attend the University of Central FL. In 2011 he graduated with a bachelor's of science in electrical engineering. While pursuing his undergraduate degree, Ricardo began working at nScript Inc. in 2010. In Januaray 2012, he began pursuit of his master's in electrical engineering at the University of Texas at El Paso. In 2013, Ricardo began to work at the U.S. Army Research Labs' Weapons and Materials Directorate (Aberdeen Proving Ground, MD) and works under an Oak Ridge Institute for Science and Education post-graduate program. There he continues his work in additive manufacturing technologies and materials, with applications in micro-fluidic devices, conformal electronics, chopped fiber reinforced composites, and sintering/melting sciences.

Permanent Address: 19225 SW 66th St.
 Pembroke Pines, FL 33332

 Or

 rodriguez.ricardo.x@gmail.com